Economic Geology
Vol. 96, 2001, pp. 453–475

New Evidence for Multiple Periods of Gold Emplacement in the Porcupine Mining District, Timmins Area, Ontario, Canada

MATTHEW D. GRAY,[†,*] AND RICHARD W. HUTCHINSON

Department of Geology and Geological Engineering, Colorado School of Mines, Golden, Colorado 80401

Abstract

The Porcupine mining district is the largest lode gold-producing district in North America, with production in excess of 62,000,000 troy oz. Nearly all of the Au has come from quartz-carbonate lode systems hosted by metamorphic rocks of greenschist facies. Field relationships and radioisotope ages of intrusions indicate that gold emplacement occurred over a span of at least 7 m.y. Depositional events that predated formation of the Timiskaming unconformity surface are manifested by auriferous clasts of detrital pyrite, banded quartz sulfide, and quartz sulfide in basal Timiskaming conglomerate. Pyritic clasts contain on average 2.54 ppm Au and are conclusive evidence for the existence of pre-Timiskaming-aged auriferous pyritic deposits. These clasts may have been derived from pyritic bodies in carbonaceous argillites of the Tisdale Group, from sulfide facies iron-formation of the Deloro Group, or from pyritic deposits of unknown genesis. Auriferous banded sulfidic quartz clasts were probably derived from iron-formation of the Deloro Group and auriferous sulfidic quartz clasts possibly from epigenetic quartz sulfide veins.

Intrusion-related and post-Timiskaming gold deposition is evidenced by Cu-Au-(Mo) mineralized porphyry and younger quartz-carbonate gold veins. The magmatism that emplaced feldspar and quartz-feldspar porphyries was accompanied by Cu-Au-(Mo) mineralization at the Dome mine, where a conformable quartz-feldspar porphyry intrusion and its host greenstones are pervasively and atypically copper and gold mineralized, and the porphyry is anomalously molybdenum enriched. A new U-Pb zircon date on this mineralized porphyry fixes its emplacement and the maximum age of Cu-Au-(Mo) deposition at 2688 ± 2 Ma. This mineralization was overprinted by later gold mineralization in the form of planar, sheeted, and en echelon auriferous quartz veins and by mineralized shear and/or fault zones. Field relationships indicate that these veins significantly postdate emplacement of the porphyries and Timiskaming sedimentation. The latest vein systems form the bulk of the ore at the Dome mine and are similar to the most economically significant veins of the district.

The largest gold deposits of the district are spatially associated with, but not in, porphyries similar to those exposed at the Dome mine. This association has led to considerable speculation regarding the genetic relationship of felsic porphyry emplacement to ore formation. The results of this study show that although some Au was deposited during a Cu-Au-Mo event temporally linked to porphyry emplacement, most of the Au at the Dome mine was emplaced significantly later than the porphyries. The documentation of at least three broad periods of Au emplacement, at least two of which are premetamorphic, is permissive and supportive of genetic hypotheses that invoke metamorphogenic remobilization of Au from earlier formed deposits. Alternatively, the coincidence of early gold enrichments and later economic concentrations may reflect a single, unidentified gold source from which successive but unrelated hydrothermal activity mobilized, transported, and deposited Au, with no direct genetic link between early and late episodes of gold deposition.

Introduction

THE PORCUPINE mining camp is the most productive lode district in North America and also lies within the world's largest and most prolific gold-producing greenstone belt, the Abitibi. Several mines remain active in the camp, and the 1999 production exceeded 500,000 oz Au. The district has been of economic and academic interest since its discovery in 1909, and hundreds of papers discuss various aspects of its geology. Excellent overviews of the district's geology are comprehensive reports of Ferguson (1968) and Pyke (1982). Other important publications include the maps and reports of Burrows (1911, 1912, 1915, 1924) and Hurst (1939); discussions of structural and geologic settings by Dunbar (1948), Davies (1977), Karvinen (1982), Hodgson (1983), Mason et al. (1988), Piroshco and Kettles (1988, 1991), and Brisbin (1997); stratigraphic descriptions by Lorsong (1975), Born (1996), and Ayer et al. (1999); petrologic, geochemical, and alteration studies by Davies and Whitehead (1980), Fyon and Crocket (1982), and Duff (1982); fluid inclusion data of Smith et al. (1984) and Walsh et al. (1988); and property-specific reports and unpublished theses on the Dome mine (Rogers, 1982; Aitken, 1988; Proudlove, 1989; Proudlove et al., 1989), the Pamour 1-Hoyle mines (Lickley, 1985; Aitken, 1990), the Hollinger-McIntyre mines (Burrows and Spooner, 1986; Mason and Melnik, 1986a, b; Mason et al., 1986; Wood et al., 1986; Melnik-Proud, 1992), the Owl Creek mine (Elliot, 1984; Kingston, 1987), and the Hoyle Pond mine (Downes et al., 1984; Brisbin, 1986; Rye, 1987).

Although the deposits of the district have been extensively studied, little consensus has emerged regarding several key points of district geology. In particular, the interrelationships among early mineralizing events, felsic porphyry emplacement, and formation of the exploited ores remain contentious. Evidence for early gold deposition in the district, which includes auriferous clasts in conglomerate, has been noted (Hutchinson and Viljoen, 1988; T. Mahoney and E. van Hees, pers. commun., 1991; Hutchinson, 1993) but not studied. The largest gold deposits of the district are spatially associated

[†] Corresponding author: e-mail, rgm_gray@terra.com.mx
[*] Present Address: Resource Geosciences de Mexico S.A. de C.V., Real #63, Col. Villa Satelite, Hermosillo, Sonora CP83200, Mexico.

with felsic porphyries, prompting considerable speculation regarding the genetic relationship of porphyry emplacement to ore formation, but research into this relationship has focused on a single deposit. Therefore, it was thought that a detailed study of mineralized clasts within ore-hosting conglomerate, coupled with a study of newly created exposures of mineralized and barren felsic intrusive rocks, might elucidate the earliest mineralizing events in the district and help define the relative timing of felsic porphyry emplacement and gold deposition. The objective was to document and temporally constrain the various gold depositional events in the district and to define the relationship of these events, if any, to felsic magmatism.

New analytical data in this study comes from differing academic and commercial sources. Precious metal and trace element analyses are from commercial (Bondar-Clegg, Swastika) and mine (Pamour 1-Hoyle, Dome) laboratories. Sulfur isotope analyses come from the laboratory of K. Shelton, Department of Geological Sciences, University of Missouri. Radiometric ages were determined using conventional U-Pb zircon geochronological methods by F. Corfu at the Jack Satterly Laboratory of the Royal Ontario Museum. Secondary ion mass spectrometry (SIMS) analyses of pyrite are by S. Chryssoulis at the Advanced Mineral Technology and Environmental Laboratory (AMTEL) at the University of Western Ontario.

Geologic Setting

The Porcupine camp lies within the Abitibi greenstone belt, a 750-km-long by 200-km-wide belt of metamorphosed volcanic, coeval subvolcanic, and intrusive rocks, locally derived clastic and chemical sedimentary rocks, and granitoid batholiths. Except for Proterozoic diabase dikes, the rocks of the Porcupine camp are entirely Archean, comprising a volcanic-dominated, volcano-sedimentary sequence. Various complex and partly contradictory stratigraphic interpretations have been suggested for the sedimentary rocks of the district (Burrows, 1924; Dunbar, 1948; Ferguson, 1968; Lorsong, 1975; Pyke, 1982; Brisbin, 1997), but here the evolved terminology of Burrows, Dunbar, and Ferguson is adopted. In this convention the Keewatin and Timiskaming Series are separated by the Timiskaming unconformity. Only those sedimentary rocks that postdate development of the Timiskaming unconformity are designated as Timiskaming. Dunbar (1948) divided the Keewatin Series into the older Deloro and younger Tisdale Groups. In general, the ca. 4,500-m-thick Deloro Group is calc-alkalic, consisting mainly of basaltic and andesitic flows in its lower part and dacitic flows and dacitic-rhyolitic pyroclastic rocks toward its top (Pyke, 1982), where discontinuous and stratigraphically stacked Algoma-type iron-formation forms a persistent stratigraphic marker. A major change in volcanism marks the base of the 4,000-m-thick Tisdale Group; the basal portion is comprised of ultramafic volcanic rocks and basaltic komatiites. This is overlain in turn by a thick sequence of distinctive, regionally continuous, variolitic, tholeiitic basalts, overlain in turn by calc-alkaline dacitic volcaniclastic rocks (Pyke, 1982). Most of the district's Au has been won from rocks of the Tisdale Group. Volumetrically minor, but economically important, porphyritic, felsic stocks (quartz-feldspar porphyry of local usage) intruded the rocks of the Tisdale Group. The largest gold deposits of the district (Hollinger-McIntyre-Coniaurum and Dome) show a clear spatial relationship to these stocks (Fig. 1). Although some Au occurs within the stocks, most of the Au in these deposits was in various lodes within the intruded basalts near the contacts with the stocks, and the genetic link, if any, between gold deposition and porphyry emplacement is contentious. Volumetrically minor alkalic albitite dikes transect the felsic porphyritic stocks, metavolcanic, and metasedimentary rocks (Hurst, 1939; Ferguson, 1968). The Archean rocks of the district have undergone regional metamorphism to lower and mid-greenschist facies. Primary textures are well preserved except where intense hydrothermal alteration and/or deformation have modified or obliterated them.

Gold in Timiskaming Conglomerate

Gold has been produced from conglomerates and argillites of the Timiskaming Series at the Broulan, Hallnor, Pamour 1, and Hoyle mines, where these strata are cut by auriferous quartz-carbonate vein systems. An important finding of this study is that in addition to the veins, Au also occurs in the conglomerate within auriferous clasts. Textural, stratigraphic, mineralogic, and geochemical data all indicate that these clasts were derived from preexisting auriferous deposits hosted by the underlying volcano-sedimentary strata and were formed, transported, and deposited by clastic sedimentary processes. These auriferous clasts constrain timing of the earliest recognized gold emplacement.

Through outcrop, drill core, and mine workings, the Timiskaming strata can be traced nearly continuously from the Dome mine in Tisdale township, 13 km northeastward to the Hoyle mine in Whitney township (Fig. 1). This belt of Timiskaming rocks is immediately north of, and follows the trace of, the Porcupine-Destor fault. A bed of conglomerate at or near the base of these strata has been a particularly productive host at the Pamour 1 and Hoyle mines where 1.849 million ounces (Moz) of Au was produced from conglomerate-hosted ore. At Dome, approximately 5.0 Moz of Au has been produced from metasedimentary rocks, chiefly marine conglomerates, which unconformably overlie Tisdale Group lavas; however, these strata differ from Timiskaming strata exposed elsewhere in the region (Holmes 1948, 1968; Roberts 1981; Pyke 1982; Proudlove, 1989; Gray, 1994) and data presented in this report suggest that the Dome conglomerates are older than the Timiskaming strata in Whitney township.

Stratigraphic relationships and description

Figure 2 shows the stratigraphic section at the Pamour 1 and Hoyle mines in Whitney township (Aitken, 1990; Kusic and Olson, 1990; West et al., 1990). This same sequence is recognized westward along strike at the Broulan and Hallnor mines (Backman, 1948; Bell, 1948). Ferguson (1968) described a similar stratigraphic section for eastern Whitney township. Although differing in details, the stratigraphic sections in Whitney township are similar, consisting of the basal Pamour conglomerate overlain by a thick sequence of fine-grained clastic sedimentary rocks. At the Pamour 1 and Hoyle mines, the basal conglomerate is stratigraphically underlain and overlain by turbiditic graywackes and thin graywacke beds are locally intercalated within the conglomerate. U-Pb

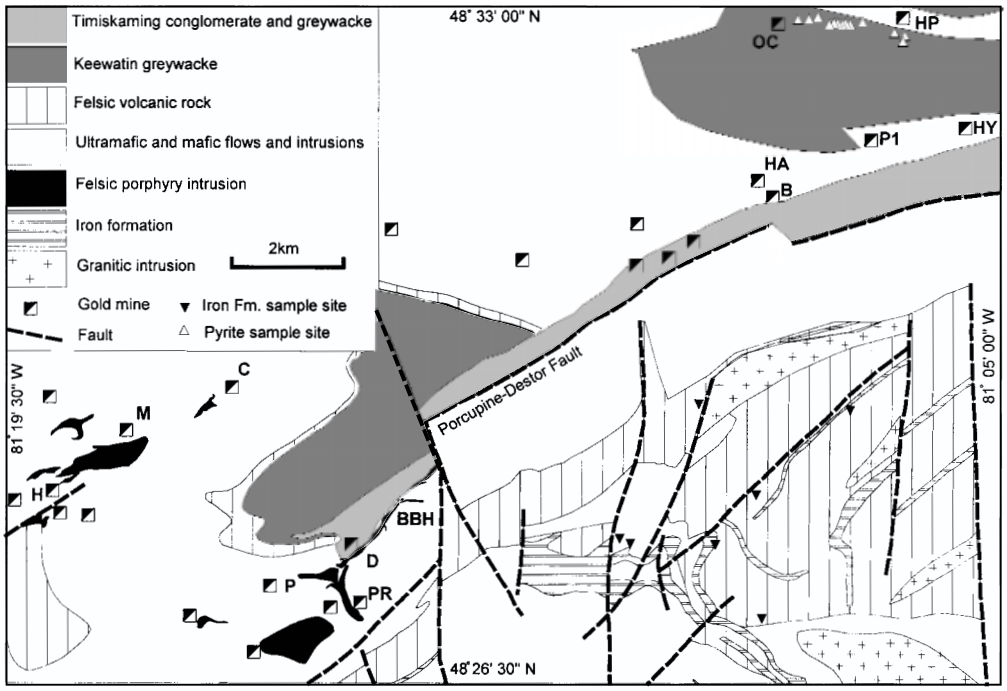

FIG. 1. Geologic map of the Porcupine mining district (compiled from Ferguson, 1968; Pyke et al., 1971; Pyke, 1982). B = Broulan, BBH = Blueberry Hill, C = Coniaurum, D = Dome, H = Hollinger, HA = Hallnor, HP = Hoyle Pond, HY = Hoyle, M = McIntyre, OC = Owl Creek, P = Paymaster, P1 = Pamour 1, PR = Preston.

age dates of detrital zircons reported by Corfu et al. (1991) are from sandstone interbeds within Pamour conglomerate (Corfu, pers. commun.) and indicate that these strata are no older than 2679 ± 4 Ma .

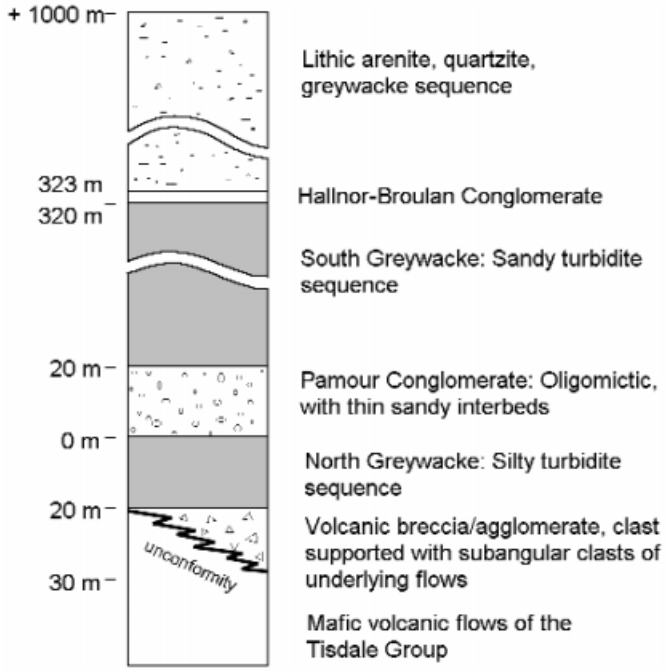

FIG. 2. Stratigraphic column for the basal Timiskaming Series, Whitney township (after Aitken, 1990; West et al., 1990).

The Pamour conglomerate is a clast-supported, poorly sorted, polymictic conglomerate, composed of approximately 85 percent clasts and 15 percent matrix, with discontinuous graywacke interbeds, 10 to 100 cm thick. Rounded, variably flattened and elongated clasts range in diameter from 5 mm to 1 m. Grading in the conglomerate was not observed at the Pamour 1 and Hoyle mines, except for rare, stratigraphically narrow bands containing extremely coarse clasts; however, Rice et al. (1992) observed poorly developed normal and reverse grading elsewhere in Whitney township. Imbrication fabric was not observed. If once present, it was probably destroyed by regional deformation that has caused rotation and flattening of clasts. The poor sorting, lack of traction bedding features, inconsistent grading, thinness, and polymictic nature of the Pamour conglomerate suggests deposition as a stacked series of subaqueous debris flows, possibly as a splay sheet to a submarine channel.

Nearly all locally exposed pre-Timiskaming rocks are represented by similar clasts in the conglomerate. Petrographically identified clasts include basalt, variolitic basalt, diorite, diorite porphyry, quartz diorite porphyry, fine- to medium-grained quartz diorite, fine-grained anorthosite, spinifex-textured ultramafic rocks, dacite, dacite porphyry, porphyritic quartz-eye rhyolite, fragmental dacite, aphanitic intermediate to felsic volcanic rocks, graywacke, quartzitic siltstone, massive chert, and white vein quartz. Sparsely present are clasts of banded sulfidic chert, massive pyrite, mixed pyrite-pyrrhotite, mixed pyrite-quartz-carbonate, and sulfidic vein quartz (Fig. 3). The clasts correspond to exposed rocks of the Deloro and Tisdale Groups and probably represent locally derived detritus. Proportions vary but mafic and ultramafic clasts predominate. No

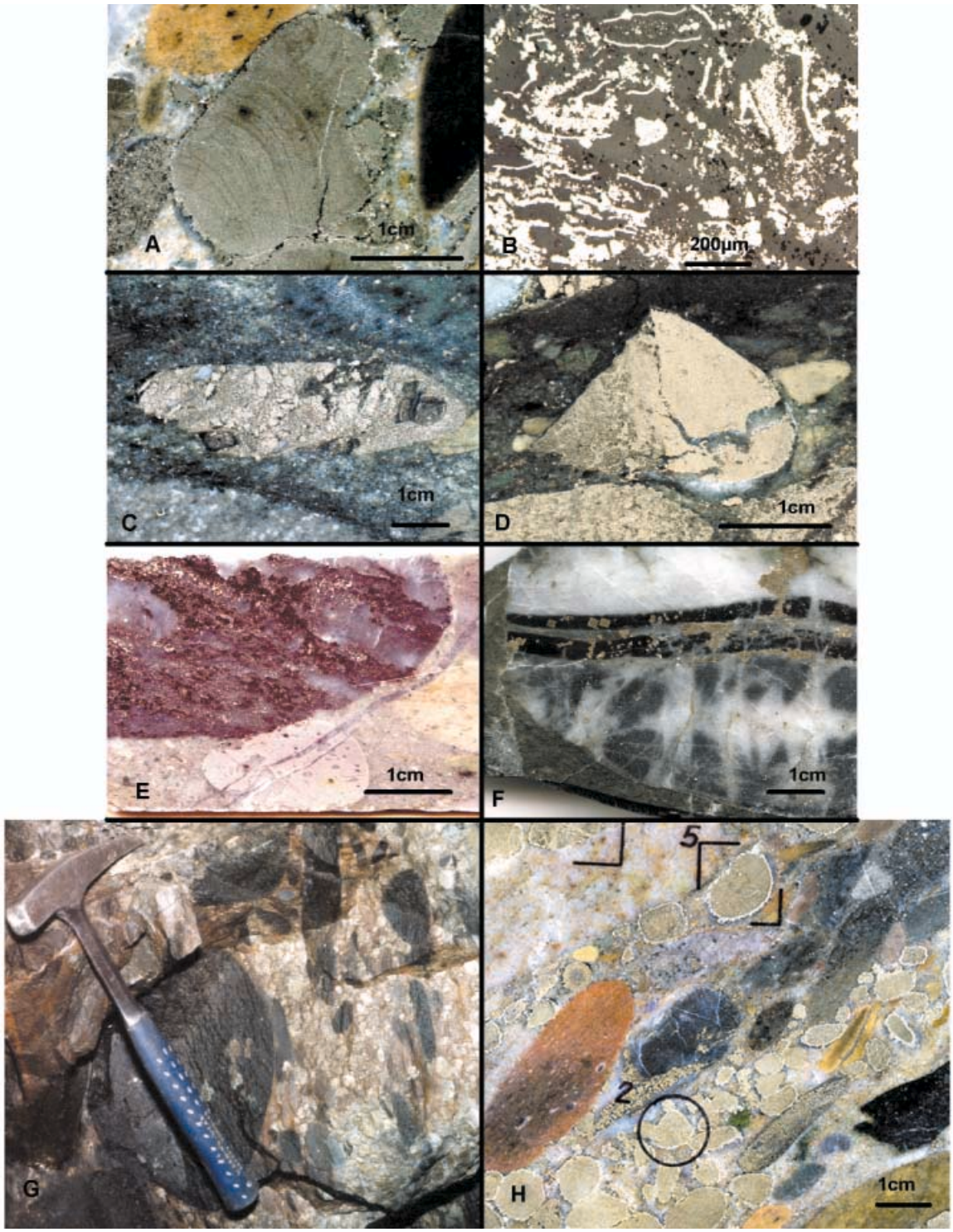

FIG. 3. Auriferous clasts in the Timiskaming conglomerate. A, C, D, E, F, and H are photographs of polished slabs. A. Pyritic clast with banding cut by clast margin. Note narrow rim of euhedral pyrite, dark basaltic clast, and honey brown andesitic porphyritic clast. B. Photomicrograph, reflected light, of irregular internal banding in pyritic clast. Light-colored areas are pyrite, darker areas are quartz and carbonate. C. Clast of semimassive pyrite. D. Angular broken pyritic clast. E. Sulfidic quartz clast. Within clast, light gray areas are quartz, dark streaks with lighter, reflective areas are fine-grained pyrrhotite. F. Banded sulfidic quartz clast containing 4.02 ppm Au. Note that banding in clast is truncated at clast margin and that anhedral and euhedral pyrite are entirely within the clast and do not extend into the conglomerate matrix. Two parallel black cherty silica bands separate granular quartz-rich upper portion from mixed quartz-carbonate in lower portion. G. Photograph of Pamour conglomerate exposed on 1422E drift, Pamour 1 and Hoyle mines. Note dark clasts of basalt and abundant, rounded, pebble-sized clasts of pyrite to right of hammer. H. Sample 1422E1DDHCUOB, showing light-colored, rounded, pyritic clasts and darker volcanic clasts. Note euhedral pyrite rims on pyritic clasts. Clasts marked were selected for SIMS analyses.

consistent variations in clast composition were noted at the Pamour 1 and Hoyle mines, and Rice et al. (1992) reported no systematic variations in clast compositions in their regional study of the conglomerate.

Matrix of the conglomerate consists of sand-sized and smaller grains of plagioclase and quartz, petrographically unidentifiable silt-clay-sized grains, and variable amounts of disseminated and/or interstitial carbonate and sericite. Most clasts and matrix have been weakly (<10 vol %) altered to sericite, carbonate, and chlorite. This alteration is ubiquitous in the conglomerate in Whitney township. It was not discerned how much of this is metamorphic and how much may represent hydrothermal alteration.

Auriferous veins in the Pamour conglomerate

Gold ore occurs in the Pamour conglomerate where it hosts numerous auriferous veins, as described by Price and Bray (1948), Aitken (1990), Kusic and Olson (1990), and West et al. (1990) at the Pamour 1 and Hoyle mines. Orebodies in the Pamour conglomerate consist of closely spaced, subparallel, quartz-dominated veins and veinlets, striking 020-040 and dipping variably to the southeast. Individual veins with subordinate carbonate and albite range from 1 to 100 cm thick and carry up to a few percent of pyrite and pyrrhotite and traces of arsenopyrite, sphalerite, chalcopyrite, and galena. Visible Au is rare in conglomerate-hosted veins. Mined orebodies consist of the veins and intervening altered and/or mineralized vein selvages. The latter rarely exceed 100 cm in width, are overprinted on the regional alteration-metamorphic mineral assemblage described above, and consist of a bleached zone with 1 to 2 percent disseminated pyrite and pyrrhotite, and variable amounts of disseminated sericite and carbonate.

Geochemical analyses for six vein samples (Table 1) include samples P14, P46, and P69 from orebodies in conglomerate and P5, P40, and P62 from isolated veins in conglomerate where vein density is too low to constitute ore. These data show that gold contents of all these veins are similar and confirm the observations of mine geologists that gold grade of an orebody is generally directly related to the amount of veining (West et al, 1990).

Auriferous clasts in the Pamour conglomerate

Gold-bearing sulfide clasts have been reported in conglomerates at the Pamour 1, Hoyle, and Dome mines (Hutchinson and Viljoen, 1988; T. Mahoney and E. van Hees, pers. commun., 1991; Hutchinson, 1993), but the clasts remained unstudied and their characteristics and occurrence undocumented. Detailed study of these clasts and their distribution in Timiskaming conglomerate was one important facet of this investigation. During this study, unreported occurrences of mineralized clasts in conglomerate were discovered in Tisdale, Whitney, and German townships, but they are best exposed in underground workings, outcrop, and drill core at the Pamour 1 and Hoyle mines, where four types of auriferous clasts were identified: pyritic, pyrrhotitic, sulfidic quartz, and banded sulfidic quartz.

Pyritic clasts: Clasts range from less than 1 cm in diameter to 5 × 15 cm. They are generally rounded (Fig. 3A, C, G, and H) but angular broken clasts were noted (Fig. 3D). Their shapes range from spherical to egg-shaped and/or elongated; the latter are oriented parallel to surrounding lithic clasts. Pyritic clasts also contain pyrrhotite, quartz, and carbonate, with minor chlorite, sericite, and tourmaline, and traces of sphalerite, chalcopyrite, galena, cassiterite, and Au. Pyrite content ranges from 30 to nearly 100 percent, the remainder consisting of up to 40 percent quartz, 35 percent carbonate, 30 percent pyrrhotite, 10 percent chlorite, 10 percent sericite, 3 percent tourmaline, 1 percent chalcopyrite, plus the above mentioned trace minerals. Typical clasts are 60 to 90 percent pyrite with 40 to 10 percent combined interstitial quartz and carbonate but only traces of pyrrhotite and chalcopyrite. Pyrrhotite and chalcopyrite are usually in contact with pyrite, but both also may occur wholly within quartz. Needles and felted aggregates of chlorite and sericite are interstitial to pyrite, usually in contact with quartz and/or carbonate. Tourmaline euhedra up to 800 μm long occur entirely within pyrite or interstitial to pyrite in contact with quartz and/or carbonate. Traces of sphalerite form anhedral blebs in quartz or pyrite, and minute galena grains (<10 μm) occur within pyrite and along its grain boundaries. A single sample contained a 1-μm rounded grain of cassiterite in pyrite. Gold siting is discussed below.

The interstitial carbonates were examined by qualitative, energy dispersive SEM X-ray analysis, typically yielding Fe peaks only, with minor Fe-Ca, and Fe-Ca-weak Mn spectral peak sets, indicating that the carbonate is impure siderite. The clasts are texturally varied. Banding is common. Some exhibit perfect concentric banding, but planar banding is clearly terminated by the clast margin in most instances (Fig. 3A). Some display irregular internal banding (Fig. 3B), while others have a porous, radial, or framboidal texture. Unbanded clasts may be massive pyrite, net-textured pyrite with interstitial quartz and carbonate, or consist of evenly distributed sulfide anhedra with interstitial quartz and carbonate. Many clasts are rimmed by selvages of euhedral pyrite up to 1 mm thick (Fig. 3A, 3H), apparently a postdepositional metamorphic or hydrothermal effect. Some clasts appear to be pyritic breccias or aggregations of pyritic nodules and semimassive pyrite in a quartz-carbonate matrix (Fig. 3C).

Pyrrhotitic, sulfidic quartz, and banded sulfidic quartz clasts: Pyrrhotitic clasts are 65 to nearly 100 percent pure, the remainder consisting of quartz with subordinate carbonate and traces of chalcopyrite, sphalerite, and sericite. Pyrrhotite forms porous, anhedral aggregates with inclusions of quartz, carbonate, and chalcopyrite, some of which appears to replace pyrrhotite along grain boundaries or microfractures. Sphalerite forms anhedral blebs in pyrrhotite, typically associated with chalcopyrite. Sericite occurs as inclusions in pyrrhotite. Margins of clasts are typically irregular and clasts are often rimmed by 150- to 400-μm-wide selvages of quartz and tourmaline.

Sulfidic quartz clasts contain less than 30 percent total sulfide in a quartz + carbonate ± sericite matrix (Fig. 3E). Pyrrhotite dominates, in amounts up to 25 percent, with up to 5 percent pyrite and traces of chalcopyrite. The sulfides form crude, poorly defined streaks and irregularly distributed patches and grains in a quartz + carbonate ± sericite matrix. The sulfide streaks are cut by clast margins.

TABLE 1. Metal Concentrations (ppm) in Quartz Veins, Conglomerate, and Conglomerate Clasts, Pamour 1-Hoyle Mine

Sample no.	Sample type	Au	Ag	Cu	Pb	Zn	Mo	As	Sb	Hg
P1BG	Congl. w/o sulfide clasts	0.01	<0.2	65	21	131	<1	2	1.4	<0.01
P11BG	Congl. w/o sulfide clasts	0.01	<0.2	42	14	73	<1	10	5.5	<0.01
P13BG	Congl. w/o sulfide clasts	0.09	<0.2	28	15	99	<1	18	2.0	<0.01
P15BG	Congl. w/o sulfide clasts	0.16	<0.2	100	22	73	<1	42	5.6	<0.01
P19BG	Congl. w/o sulfide clasts	0.02	<0.2	63	23	145	<1	90	8.5	<0.01
P21BG	Congl. w/o sulfide clasts	0.02	<0.2	25	25	294	<1	8	1.4	<0.01
Average		0.05	<0.2	54	20	136	<1	28	4.1	<0.01
Standard deviation		0.06		28	4	83		33	2.9	
P5	Quartz vein	4.54	<0.2	26	19	133	2	3580	7.3	0.02
P14	Quartz vein	10.75	<0.2	51	10	7	2	5080	10.0	0.20
P40	Quartz vein	3.99	<0.2	25	16	34	<1	1320	<1	0.02
P46	Quartz vein	4.93	<0.2	48	9	48	3	153	0.5	0.01
P62	Quartz vein	4.12	<0.2	70	8	62	<1	46	0.7	0.01
P69	Quartz vein	1.48	<0.2	44	5	29	3	30	0.6	0.01
Average		4.97	<0.2	44	11	52	2	1702	3.4	0.05
Standard deviation		3.08		17	5	44	1	2146	4.2	0.08
DDH 14529 58	Pyritic clast	1.56	3.6	556	317	42	<1	933	104.0	0.09
H1406 294'2"	Pyritic clast	3.74	2.0	364	168	51	<1	811	69.1	0.11
H1408 171'2"	Pyritic clast	2.80	3.3	316	273	38	<1	820	151.0	0.05
P1	Pyritic clast	2.07	4.2	96	191	70	<1	279	125.0	0.06
P11G	Pyritic clast	2.43								
P11PG	Pyritic clast	3.46								
P13	Pyritic clast	0.95	0.4	60	46	60	2	149	7.7	0.02
P1417MC2	Pyritic clast	1.85								
P1422E1	Pyritic clast	1.54								
P1422E1DDHCOUB	Pyritic clast	1.05	1.4	112	82	45	<1	639	50.2	0.05
P1422E2	Pyritic clast	2.37								
P1422E2DDHCO	Pyritic clast	8.45	2.0	574	129	50	<1	746	77.7	0.10
P1422E3	Pyritic clast	3.15								
P1422E3DDHCO	Pyritic clast	1.10	8.3	100	135	38	<1	622	50.1	0.12
P1422E4	Pyritic clast	2.13								
P15G	Pyritic clast	3.43								
P19B	Pyritic clast	3.01								
P19G	Pyritic clast	2.40								
P21G	Pyritic clast	2.43								
T2G	Pyritic clast	0.96								
Average		2.54	3.2	272	168	49	1	625	79.4	0.07
Standard deviation		1.64	2.4	212	92	11		275	45.9	0.03
P1417MC1	Pyrrhotitic clast	1.34								
P1417MC3	Pyrrhotitic clast	0.41								
P1417MC4	Pyrrhotitic clast	6.84								
Average		2.86								
Standard deviation		3.48								
P55	Sufidic quartz clast	1.16	<0.2	62	31	23	4	35	0.9	<0.01
PTS 10	Sufidic quartz clast	0.19	0.7	877	35	433	<1	182	4.6	0.02
P71	Banded quartz clast	4.02	1.1	137	12	17	4	155	2.3	0.01
DDH 14935 197.7	Overprinted clast	>10.00								
P36G	Overprinted clast	14.56	24.0							
P45G	Overprinted clast	15.82	12.0							

Notes: Mo and Sb analyses below detection limit were set to detection limit for calculation of averages and standard deviations; congl. w/o sulfide clasts = conglomerate sample without sulfide clasts

Banded sulfidic quartz clasts are 60 to 98 percent quartz with subordinate carbonate, pyrrhotite, pyrite, and minor chlorite, sericite, magnetite, tourmaline, chalcopyrite, and sphalerite. Banding is defined by sulfide-, carbonate-, and magnetite-rich layers and by variations in color of quartz (Fig. 3F). These parallel bands are cut by clast margins.

Distribution of auriferous clasts

Auriferous pyritic clasts occur in distinct, conformable, stratiform and strata-bound layers within the conglomerate, which range up to 2 m in stratigraphic thickness but generally are no more than 0.3 m thick. These layers generally contain 2 to 5 percent, but in places up to 40 percent, of pyritic clasts (Fig. 3G, 3H). The layers are continuous and form mappable local marker beds. They are particularly well exposed on the 1400 level of the Pamour 1 and Hoyle mines, where an exploration-haulage drift and crosscuts transect these strata. In the 1422E drift, an individual pyritic clast-bearing layer has been continuously traced along strike for more than 200 m, and two drill holes indicate that it extends updip at least 155 m and downdip at least 65 m. This layer coincides exactly with an exceptionally coarse conglomerate bed, containing boulders up to 1 m in diameter of fine- to medium-grained quartz diorite and anorthositic gabbro (Fig. 4). The extremely coarse bed is continuously traceable. The pyritic clasts within it occur both stratigraphically above and below the boulders. A second, finer pyritic clast-bearing layer on the 1400 level is continuously traceable for a minimum strike length of 160 m, and seven drill holes indicate a minimum up- and/or downdip extent of 170 m. Lack of exposure, however, obscures the total extent of these layers.

Similar bands containing pyritic clasts were mapped and sampled in the 1417 and 10258 midcuts. These exposures, plus sparse drilling data, show that auriferous pyritic clasts are widespread within the Pamour conglomerate, distributed over a minimum strike length of 880 m with a minimum up- and/or downdip extent of 260 m. The pyrite clast-rich layers occupy particular stratigraphic levels and are spatially unrelated to veining, structures, or orebodies. Together with clast morphology and textures, these relationships clearly indicate that the pyritic clasts were detrital in origin.

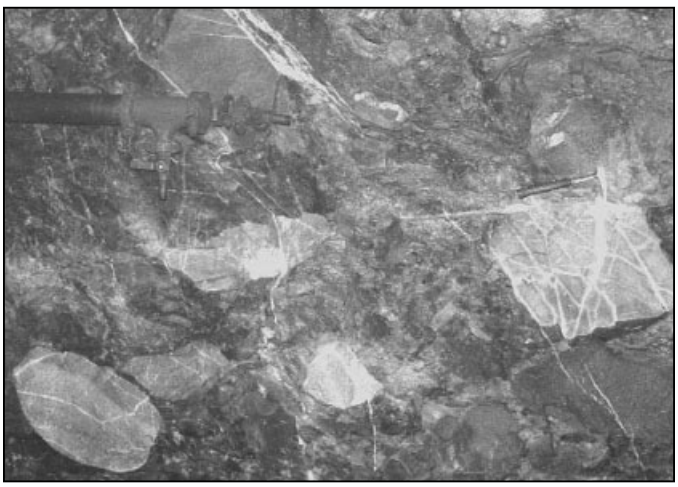

FIG. 4. Photograph of exceptionally coarse conglomerate bed with abundant pyritic clasts, exposed in 1422E drift, Pamour 1 and Hoyle mines. Drift wall is parallel to strike of bed and cuts it at an oblique angle. Pyritic clasts are not visible at this scale but are present throughout the rib face. Note metamorphic white quartz veins cut both the boulders and the conglomerate matrix. These veinlets are up to 5 cm thick where they cut boulders but are only a few millimeters thick where they cut conglomerate matrix.

Unlike the pyritic ones, pyrrhotitic clasts are not associated with particular stratigraphic levels in the Pamour conglomerate but are sporadically distributed throughout the conglomerate, not occurring in mappable or continuous layers. They are variably distributed through a minimum vertical extent of 550 m between the 1000 and 2400 levels and a minimum strike length of +2,000 m from the Pamour 1 shaft to the 7-264 exploration drift. Their distribution closely coincides with that of orebodies and auriferous veins. These relationships and the textures of the clasts suggest strongly that pyrrhotitic clasts formed by replacement processes accompanying vein formation. Near ore and alteration zones, both pyritic and normal lithic clasts were affected by this process.

Sulfidic quartz and banded sulfidic quartz clasts occur ubiquitously but sporadically and sparsely throughout the conglomerate. They exhibit no affinities to veins or orebodies and lack replacement textures, evidence that these clasts, too, are of detrital origin.

Geochemical analyses of auriferous clasts

Gold and multielement analyses of the three different types of detrital auriferous and pyrrhotitic replacement clasts are presented in Table 1. Clast size permitting, individual clasts were diamond sawed from slabbed samples. Pyritic clasts were also extracted by coarsely crushing (+3 cm) conglomerate, bathing the product in hydrofluoric acid to dissolve silicates, and manually separating pyritic clasts. Resulting samples comprised 10- to 30-g composites of many pyritic clasts from the same hand specimens. Gold contents were determined by standard fire assays with atomic absorption finish. For some samples, Ag, Cu, Pb, Zn, and Mo were analyzed by ICP using HCl/HNO_3 extraction, As and Sb by neutron activation, and Hg by cold vapor atomic absorption with HCl/HNO_3 extraction. For others, Ag, Cu, Pb, Zn, and Sb were determined by atomic absorption with aqua regia extraction. The content and distribution of Au and As in individual pyritic clasts was determined by SIMS analyses.

Six background samples of conglomerate free of pyritic clasts were obtained from the same hand specimens as the pyritic clast composites. All were analyzed and resulting data (Table 1) indicate that the pyritic clasts are strongly gold enriched relative to the host conglomerate.

Pyritic clasts from conglomerate outside of ore zones lack evidence of later epigenetic overprinting yet are consistently auriferous, ranging from 0.95 to 8.45 ppm Au and averaging 2.54 ppm (Table 1). Gold contents are also remarkably uniform in this sample set, with 16 of the 20 samples containing between 1.0 and 3.5 ppm. Moreover, gold contents in pyritic clasts from conglomerate remote from orebodies and auriferous veins are similar to those in pyritic clasts from proximal samples. Pyritic clasts are also enriched in As and Sb, averaging 625 and 80 ppm, respectively. Ag, Cu, Pb, and Zn are not significantly enriched.

The average gold content of pyrrhotitic clasts, 2.86 ppm, is comparable to that of pyritic clasts, but unlike the latter, the

former are variably gold enriched. In the three samples analyzed, contents range from 0.41 to 6.84 ppm Au. Unpublished mine assay data yielded low and high assays of 0.17 and 21.44 ppm Au, respectively, for the pyrrhotitic clasts (E. van Hees, 1993). Multielement data are not available for the pyrrhotitic clasts. Two samples of sulfidic quartz clasts contained 0.19 and 1.16 ppm Au. One banded sulfidic quartz clast assayed 4.02 ppm Au with elevated As. Textures in pyritic clasts from conglomerate within orebodies are described in the following section, and they indicate an overprinting of late gold mineralization. Compared to others, these clasts are extremely enriched in Au and Ag and contain, on average, a minimum of 13.46 ppm Au and 18 ppm Ag.

Gold occurrence in auriferous clasts

The siting of Au within auriferous clasts from conglomerate within and beyond orebodies was studied, using petrography, SEM imaging, and SIMS studies. Pyritic clasts within orebodies differ from those outside. The former host native gold grains up to 50-μm diameter within the euhedral pyrite that rims the clasts, exhibit abnormally high silver and gold contents relative to the latter (Table 1), and are surrounded by gold-bearing euhedral pyrite grains disseminated in intensely altered conglomerate matrix. This indicates that some of the Au in pyritic clasts within orebodies is not primary but reflects late introduction of Au, probably related to the veining and alteration that formed the host orebodies. All samples collected within orebodies were therefore considered to have undergone late introduction of Au, thus were treated as a separate population during statistical evaluation of geochemical data.

Gold in pyritic clasts collected outside of orebodies occurs as 1- to 6-μm grains along pyrite grain boundaries (Fig. 5A), within grains (Fig. 5B), sometimes in contact with chalcopyrite, and as submicroscopic Au within pyrite. The micron-sized gold grains often lie along pyrite grain boundaries, but their distribution is not spatially related to clast margins. The gold grains identified by SEM are insufficient to account for the analyzed gold content of the samples. Five pyritic clasts from hand specimen 1422E1DDHCUOB (Fig. 3H) were selected for SIMS analysis to test for the presence of submicroscopic Au in solid solution in pyrite. This specimen was from barren conglomerate outside of any known ore zone. A composite sample of its pyritic clasts assayed 1.05 ppm Au. Table 2 shows the results of 70 individual 15-μm spot SIMS analyses for Au and As on three different types of pyrite: euhedral pyrite that forms clast rims, internal medium-grained pyrite, and internal fine-grained pyrite.

The euhedral pyrite from clast rims averages 0.80 ppm Au, clearly less than both medium-grained (avg 1.10 ppm Au) and fine-grained pyrite (avg 1.58 ppm Au) from clast interiors. Scatterplots (Fig. 6) show a positive correlation between Au and As in the fine- and medium-grained internal pyrite, whereas the gold content in the euhedral pyrite is uniformly low, independent of arsenic content. Discrete gold grains were not detected by SIMS analyses. This, together with the positive correlation between Au and As in both types of internal pyrite, indicates that Au in the internal pyrite is in solid solution and was incorporated into the pyrite when the latter first formed. The relatively uniform and lower gold contents of euhedral pyrite in the clast rims are best explained by loss of Au during metamorphic recrystallization of auriferous pyrite.

Sources of auriferous clasts

In an attempt to identify possible sources of the auriferous pyritic clasts, their textural and geochemical characteristics were compared to those of known auriferous pyritic occurrences that predate deposition of the conglomerate and thus may have served as their source. The auriferous pyritic clasts were also similarly compared to the whole vein samples from the auriferous veins that transect the Pamour conglomerate. A lack of multielement analytical data precluded similar comparison of sulfidic quartz, banded sulfidic quartz, and pyrrhotitic clasts to known mineral occurrences.

The textures and mineralogy of the pyritic clasts resemble those of nodular and massive pyrite occurrences hosted by Deloro Group iron-formation (Pyke, 1982) and Tisdale Group interflow carbonaceous strata. Examples of the former are exposed in Whitney township, the latter at the Hollinger, Moneta Porcupine, and Coniaurum mines in Tisdale township (Buffam, 1968; Carter, 1968; Jones, 1968) and at the Owl Creek and Hoyle Pond mines in Hoyle township (Elliot, 1984; Brisbin, 1986; Rye, 1987). To enable geochemical comparisons between the clasts and these preexisting pyritic strata, these two possible sources were sampled and analyzed.

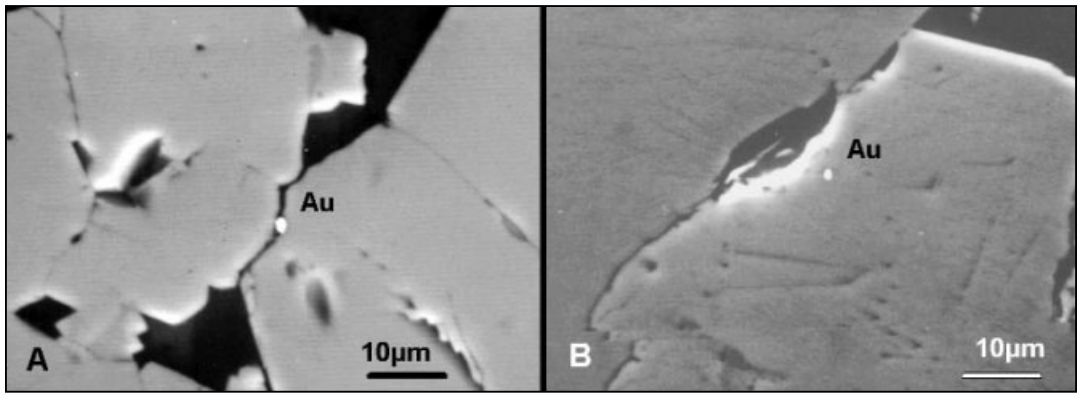

FIG. 5. SEM images of gold (Au) in pyrite along pyrite grain boundary (A) and within pyrite (B). Light-colored area along grain boundary left of Au grain in B is an edge reflection.

TABLE 2. Secondary Ion Mass Spectrometry (SIMS) Analyses of Pyritic Clasts

Clast	Spot	Location	Pyrite type	Au (ppm)	As (ppm)
2	67	Edge	Euhedral rim	0.56	269
2	68	Edge	Euhedral rim	0.98	600
2	69	Edge	Euhedral rim	0.39	1104
2	71	Edge	Euhedral rim	1.09	944
2	81	Edge	Euhedral rim	0.30	529
2	82	Edge	Euhedral rim	0.53	574
3	17	Edge	Euhedral rim	0.99	528
3	18	Edge	Euhedral rim	0.87	682
3	22	Edge	Euhedral rim	0.94	669
4	30	Edge	Euhedral rim	0.41	163
4	35	Edge	Euhedral rim	0.46	519
5	42	Edge	Euhedral rim	0.84	337
5	43	Edge	Euhedral rim	0.87	358
6	4	Edge	Euhedral rim	0.65	392
6	6	Edge	Euhedral rim	0.87	298
6	44	Edge	Euhedral rim	0.82	979
6	45	Edge	Euhedral rim	1.08	1131
6	46	Edge	Euhedral rim	0.82	865
6	47	Edge	Euhedral rim	0.96	863
6	48	Edge	Euhedral rim	1.03	947
6	49	Edge	Euhedral rim	1.30	1250
Average				0.80	667
2	66	Edge	Interior medium grained	0.73	442
2	70	Edge	Interior medium grained	0.83	820
2	73	Interior	Interior fine grained	2.56	1063
2	74	Interior	Interior fine grained	1.84	1335
2	75	Interior	Interior fine grained	3.46	1385
2	76	Interior	Interior fine grained	2.97	1243
2	77	Interior	Interior fine grained	2.54	1089
3	15	Edge	Interior fine grained	1.85	769
3	16	Edge	Interior fine grained	1.40	817
3	19	Edge	Interior medium grained	1.25	647
3	20	Edge	Interior medium grained	1.14	799
3	21	Edge	Interior medium grained	0.96	766
4	31	Edge	Interior medium grained	0.29	352
4	32	Edge	Interior medium grained	0.38	475
4	33	Edge	Interior medium grained	0.46	693
4	34	Edge	Interior medium grained	0.46	693
5	23	Interior	Interior fine grained	0.96	788
5	36	Interior	Interior fine grained	0.59	924
5	37	Interior	Interior fine grained	1.33	523
5	38	Interior	Interior fine grained	2.74	927
5	39	Edge	Interior medium grained	1.09	787
5	40	Edge	Interior medium grained	1.08	478
5	41	Edge	Interior medium grained	3.27	644
5	23a	Interior	Interior fine grained	0.90	537
6	1	Edge	Interior fine grained	1.72	347
6	2	Edge	Interior fine grained	1.56	431
6	3	Edge	Interior fine grained	1.19	443
6	5	Edge	Interior medium grained	1.11	497
6	50	Interior	Interior fine grained	1.01	1102
6	51	Interior	Interior fine grained	0.93	740
6	52	Interior	Interior fine grained	1.04	1090
6	53	Interior	Interior fine grained	1.50	688
6	54	Interior	Interior fine grained	0.94	1034
6	55	Interior	Interior fine grained	1.10	1011
6	56	Interior	Interior fine grained	0.78	655
6	57	Interior	Interior fine grained	0.97	735
6	58	Interior	Interior medium grained	1.58	769
6	59	Interior	Interior medium grained	1.47	670
6	60	Interior	Interior fine grained	1.38	759
6	61	Interior	Interior medium grained	0.86	613
6	62	Interior	Interior medium grained	1.07	723
6	63	Interior	Interior medium grained	1.54	713
6	64	Interior	Interior medium grained	1.00	745
6	65	Interior	Interior medium grained	1.39	686
Average				1.35	760

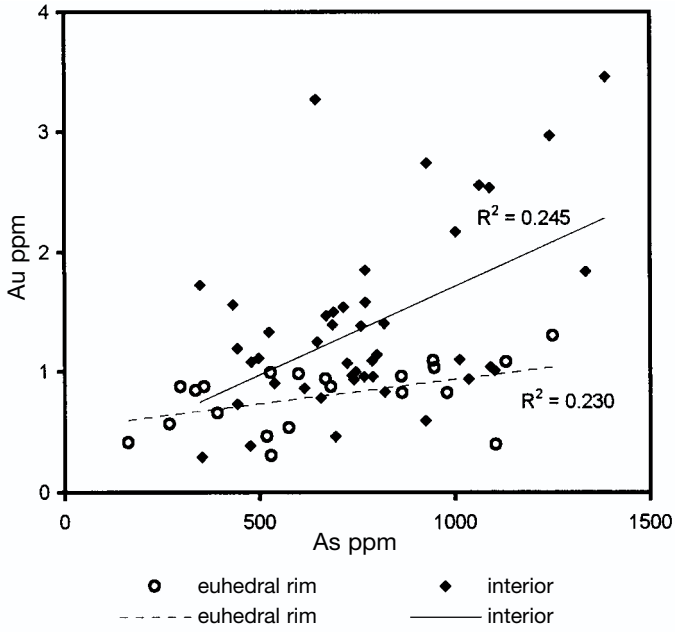

FIG. 6. Scatter plot with linear regression lines showing relationship between As and Au contents for internal and euhedral rim pyrite, as determined by SIMS analyses.

Because it was desired to determine primary gold contents in these rocks, samples were collected only from localities not associated with any known epigenetic mineralizing event. Gray (1994) presented evidence to this effect, but district-wide low-intensity alteration prevents unequivocal proof of this condition. Fifteen samples of iron-formation and 14 samples of pyritic interflow strata were collected from drill core from Whitney and Hoyle townships (Fig. 1). The multielement analytical data (Table 3, App. 1) show that, geochemically, the pyritic clasts are similar to pyrite from carbonaceous sedimentary strata of the Tisdale Group except for a 6× greater gold content and somewhat lower Zn and Hg contents. Both sample sets exhibit similar contents of Ag, Cu, Pb, Mo, As, and Sb, and similar As/Sb ratios. Pyritic clasts are, however, geochemically distinct from sulfide facies iron-formation of the Deloro Group. They are 28× richer on average in Au than the latter, contain higher Cu, Pb, As, Sb, and Hg, but lower Ag and Zn, and exhibit dissimilar As/Sb ratios.

Pyritic clasts are also geochemically dissimilar to auriferous veins in the Pamour conglomerate (Tables 1 and 3). The low sulfide content of these veins prevented preparation of sulfide separates large enough for multielement geochemical analyses. However, whole vein samples were analyzed and the resulting metal ratios are thought to reasonably reflect the relative contents and proportions of metals within the sulfides of these veins. These auriferous veins have distinctively high As/Sb ratios, averaging 457, which contrasts markedly with average As/Sb ratios of 10 in the pyritic clasts (Table 3). Comparison of Au/Ag ratios is of questionable significance because Ag was not present above the detection limit of 0.2 ppm in vein samples, yielding ratios of infinity. However, it is significant that, although not detectable in vein samples, Ag was detectable in more than half of the pyritic clasts analyzed. If

Table 3. Geochemical Comparison of Pyritic Clasts and Possible Source Rocks

Sample group	*n*	Au	Ag	Au/Ag	Cu	Pb	Zn	Mo	As	Sb	As/Sb	Hg
Interflow pyrite	4	0.42	3	0.2	233	144	419	1	563	74	11	0.635
SIF	12	0.09	7	0.1	62	85	601	2	176	8	35	0.088
Veins	6	4.97	0.2	24.8	44	11	52	2	1702	3	457	0.046
Pyritic clasts	20 (8)	2.54	3.2	1.4	272	168	49	1	625	79	10	0.074

Notes: All assays reported in ppm; interflow pyrite = pyrite concentrates from carbonaceous sedimentary horizons, Tisdale Group, Hoyle township; SIF = samples from sulfide facies iron-formation, Deloro Group, Whitney township; veins = vein samples from the Pamour conglomerate, Whitney township; and pyritic clasts = clasts from the Pamour conglomerate, Whitney township; for pyritic clasts n = 20 for Au analyses, n = 8 for other metals

Ag contents are arbitrarily standardized at the detection limit, vein samples have an average Au/Ag ratio of 24.8, whereas pyritic clasts have an average Au/Ag ratio of 1.4, an order of magnitude difference. Comparison of sulfur isotope data for 11 pyritic clast samples and nine vein pyrite samples did not allow for statistically meaningful separation of the two populations, but vein pyrite (avg δ^{34}S 1.84‰) is consistently lighter isotopically than pyrite from clasts (avg δ^{34}S 3.07‰). The geochemical dissimilarity between the auriferous pyritic clasts and auriferous veins precludes formation of the pyritic clasts by replacement processes associated with vein formation but is consistent with their detrital origin.

The pyritic clasts are texturally and geochemically most similar to pyritic nodules and massive pyrite lenses in interflow argillites of the Tisdale Group. Similar pyritic deposits are, therefore, the most likely source for the detrital pyritic clasts, but derivation from auriferous sulfide facies iron-formation or auriferous pyritic deposits of unknown nature cannot be ruled out. The lack of chalcopyrite- and sphalerite-rich clasts and the high gold content of the pyritic clasts suggest that the latter were not derived from polymetallic volcanogenic massive sulfide deposits like Kidd Creek, Kamkotia, and others in felsic rocks of the Deloro or Tisdale Groups. The distribution, morphology, and textures of the clasts, combined with their contrasting geochemical characteristics with the auriferous veins, clearly indicate that the clasts did not form by replacement processes accompanying vein formation.

Geochemical data permitting comparison of sulfidic quartz clasts to known mineral occurrences are insufficient for determining their origin. However, textures of these clasts are similar to those in many auriferous sulfidic quartz veins, and this parentage is here preferred. Such veins may be related to pre-Timiskaming magmatic activity evidenced by ultramafic, monzonitic, and granodioritic intrusions in the Deloro Group. Geochemical data permitting comparison of banded sulfidic quartz clasts to known mineral occurrences are also insufficient for determining their origin. The banded textures and mineralogical composition of these clasts, however, are remarkably similar to those of iron-formations of the Deloro Group, and this derivation is here suggested. Textural and field relationships indicate a replacement origin for pyrrhotitic clasts, rather than derivation from an earlier sulfide body.

Mineralized and Barren Porphyries of the Dome Mine

Mineralized and barren porphyritic felsic intrusions crop out between the Dome 8 shaft and the abandoned Ontario Northland Railroad tracks to the northeast, in an area encompassing the recently developed Blueberry Hill pit, a quarry, and the Foley O'Brien claims (Fig.1, 7). The area was chosen for study because ore-hosting porphyritic felsic bodies are present and extensive geological and geochemical data have very recently become available for it through surface exploration stripping, pit development, and diamond drilling. The geology of this area was mapped and discussed by Hurst (1939), Ferguson (1968), Rogers (1982), and Aitken (1988). Portions of the property were remapped at scales of 1:360 and 1:600 (Gray,1994) and the resulting new observations are discussed below.

This area is underlain by a series of northeast-striking, north-dipping, south-topping, mafic volcanic flows. The northwestern contact of this sequence of mafic flows is an unconformity that juxtaposes conglomerate, graywacke, and argillite against the flows (Fig. 7). These strata have been assigned a Timiskaming age (Hurst, 1939; Ferguson, 1968; and Brisbin, 1997). A small body of fine- to medium-grained plagioclase- and orthopyroxene-bearing, gabbroic porphyry crops out in sharp contact with mafic flows in the south. A medium-grained, magnetite-rich, pyroxenitic intrusion is exposed in a quarry northeast of the Blueberry Hill pit, where fine-grained mafic intrusions are also exposed. None of these small intrusions are shown in Figure 7 as they are not apparently relevant to the problem under investigation.

Felsic porphyritic rocks crop out in a generally conformable, northeast-trending belt parallel to the volcanic strata at, or immediately south of, the Timiskaming unconformity and also as west- and northwest-striking bodies that transect the volcanic flows. Traditionally, these bodies have been mapped as undifferentiated quartz-feldspar porphyry (Holmes, 1968; Rogers, 1982; Aitken, 1988), were termed "Preston Porphyry" in local usage, and ascribed a post-Timiskaming age. An important result of this study is the clear documentation that the conformable and unconformable felsic porphyritic bodies are lithologically distinct, although probably products of related, yet different intrusive activity. Furthermore, crosscutting field relationships among these differing felsic porphyries, structural features, and mineralized zones all serve to constrain the relative timing and lithologic affiliations of gold mineralization.

Two distinct varieties of porphyry were identified; quartz-feldspar porphyry and feldspar porphyry, both silica saturated, variably quartz and feldspar porphyritic, lacking in potassium feldspar, and of porphyritic-aphanitic texture. Although similar in whole-rock composition (App. 2), the two have distinctly different modes of occurrence, accessory mineral assemblages, and trace element geochemical signatures. Petrographically quartz-feldspar porphyry is clearly different

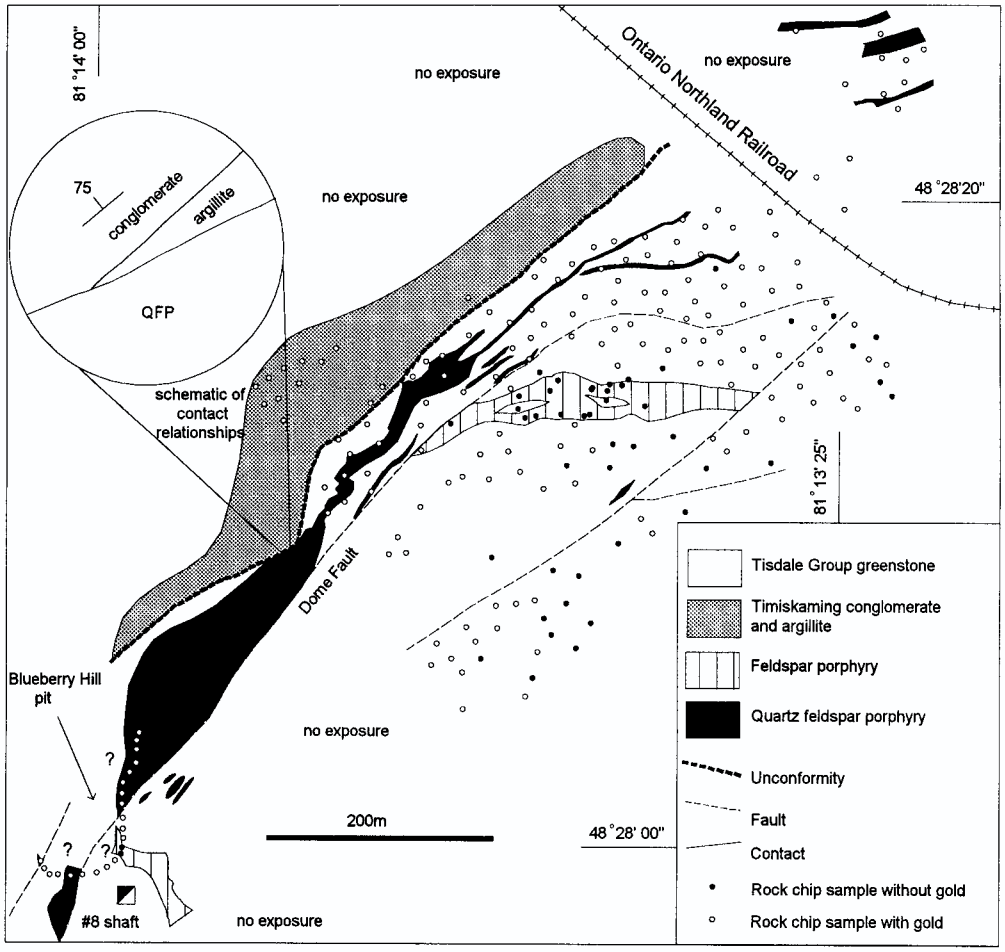

FIG. 7. Geologic map of the Blueberry Hill-Foley O'Brien area (compilation of unpub. mine maps of McCulloch (1948) and Hunt (1993) and mapping by the authors). Rock chip sample sites without gold do not contain gold above a 0.005 ppm detection limit.

from feldspar porphyry, however, in hand specimens and outcrops, due to the effects of low-rank metamorphism and hydrothermal alteration, the differences are not always readily distinguishable. In the field, both weather to light gray to white, and their porphyritic texture is variably discernible depending upon the degree of alteration. On fresh surfaces both range from light gray to blue- and green-gray. Quartz phenocrysts are usually discernible in hand specimens but plagioclase phenocrysts often cannot be distinguished from the groundmass. These megascopic similarities probably explain why the two types have not been previously distinguished.

Quartz-feldspar porphyry is holocrystalline, hypidiomorphic-inequigranular, porphyritic-aphanitic, with a phenocryst/groundmass ratio of approximately 50/50. The dominant phenocrysts (Fig. 8A) are quartz (5–30%) and oligoclase (95–70%), and average modes are about 10 percent quartz, 90 percent oligoclase. Quartz phenocrysts are rounded, subhedral and equant, 100 to 4000 μm in diameter but generally less than 2,500 μm. Large grains with highly embayed-scalloped margins, interpreted as resorption textures, are common. Oligoclase forms anhedral to euhedral equant grains and laths 200 to 4,000 μm in diameter and length. Accessory zircon euhedra 40 to 100 μm long occur as inclusions in oligoclase and groundmass. The groundmass is composed of 10- to 50-μm granular quartz and untwinned plagioclase. Disseminated clots of opaque Fe oxides, sometimes associated with chlorite, may represent relict mafic phenocrysts.

Feldspar porphyry is holocrystalline, hypidiomorphic-inequigranular, porphyritic-aphanitic, with a phenocryst/groundmass ratio of approximately 55/45. The dominant phenocrysts (Fig. 8B) are oligoclase (>99%) and rare quartz (<1%). The latter form rounded, subhedral, equant grains, 100 to 3,000 μm in diameter. The former are subhedral to euhedral equant grains and laths 200 to 4,000 μm in diameter. Accessory apatite euhedra in the groundmass are up to 1,000 μm long. Accessory zircon occurs as inclusions in oligoclase. The groundmass is comprised of 10- to 50-μm granular quartz and untwinned plagioclase. No mafic minerals were identified; any originally present were probably destroyed by hydrothermal alteration.

Both porphyries are pervasively hydrothermally altered to mineral assemblages similar to those associated with lode gold deposits throughout the district. The characteristic alteration minerals, in order of decreasing abundance, include sericite, carbonate, quartz, chlorite, pyrite, chalcopyrite, tourmaline, sphalerite, and fuchsite. Sericite is ubiquitous and

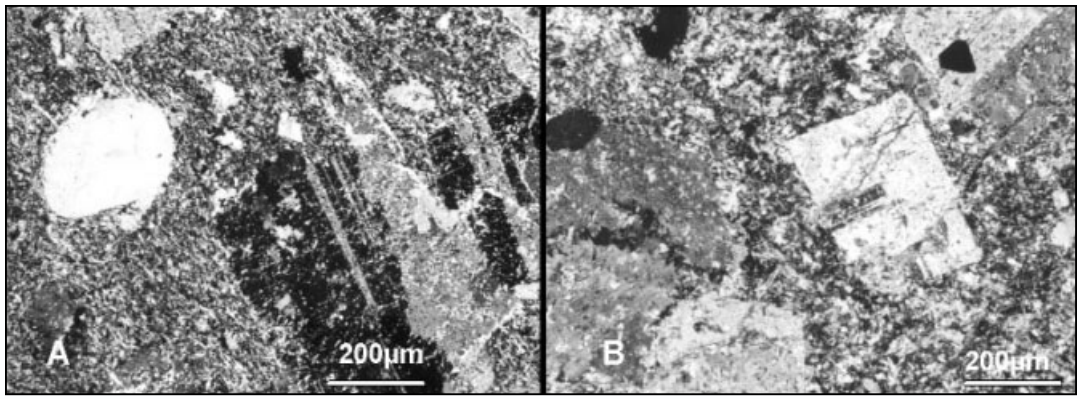

FIG. 8. Photomicrographs, crossed polars. A. Quartz-feldspar porphyry, note rounded quartz phenocryst and intensely sericitized plagioclase and groundmass. B. Feldspar porphyry. Note dark rounded apatite grain at left edge of image, triangular opaque pyrite grain in upper right, and intensely sericitized plagioclase and groundmass.

ranges in amount from 5 to 50 vol percent. Carbonate alteration is also ubiquitous, ranging from 3 to 20 vol percent. Siliceous alteration is common but not ubiquitous, manifested as microveinlets of quartz, sometimes with carbonate, sericite, pyrite, chalcopyrite, plagioclase, and/or tourmaline. Quartz microveinlets generally comprise <2 vol percent of the rock. Chlorite comprises up to 3 percent of the rock, as disseminations and radiating clusters in the groundmass, clots in the core of plagioclase phenocrysts, in discontinuous chloritic microveinlets, in sulfide lenses, and as a component of sericitic microveinlets. Tourmaline is present in pyritic veinlets and as traces in sericitic and/or carbonate veinlets. Rare fuchsite occurs in sericitic microveinlets. Disseminated pyrite in trace amounts is ubiquitous in both quartz-feldspar porphyry and feldspar porphyry, but in quartz-feldspar porphyry pyrite is also present in microveinlets with tourmaline and chalcopyrite, with or without associated quartz, carbonate, and sericite, and in semimassive lenses, up to 40 cm wide and several meters long, with chlorite, and lesser chalcopyrite, quartz, carbonate, and sericite. Chalcopyrite is ubiquitous in quartz-feldspar porphyry and uncommon in feldspar porphyry. In quartz-feldspar porphyry it is present as disseminations, as a constituent of the pyritic microveinlets, and as segregations in the pyritic lenses described above. In feldspar porphyry only traces of disseminated chalcopyrite were found, and these in less than 30 percent of the samples examined. Traces of sphalerite are associated with chalcopyrite in both quartz-feldspar porphyry and feldspar porphyry. Increased intensities of sericitic, carbonate, and chloritic alteration do not correlate with greater gold contents, but total pyrite content and Au are weakly positively correlated.

The two porphyries have distinctly different modes of occurrence. Quartz-feldspar porphyry crops out in a northeast-striking, conformable zone, but its contacts with greenstone are locally discordant (Fig. 7). Xenoliths of greenstone in quartz-feldspar porphyry indicate that it intruded the greenstones. The contact between quartz-feldspar porphyry and the sedimentary strata crops out at only one locality, where the quartz-feldspar porphyry contact transects sedimentary bedding at oblique angles. The contact is sharp and appears to be intrusive, but the possibility that the contact is structural and related to deformation associated with the Dome fault cannot be ruled out. Xenoliths of argillite in quartz-feldspar porphyry are common and are similar to the locally exposed argillite, but they may be derived from argillites intercalated within older flows of the Tisdale Group. In the Blueberry Hill pit, the quartz-feldspar porphyry is 80 m thick but thins to the northeast, and in the Foley O'Brien claims crops out as a series of interfingering, subparallel, conformable lenses (Figs. 7, 9). This belt of porphyry exposures is continuously mappable for 500 m northeastward across the Foley O'Brien claims. Here its outcrop pattern may reflect some later structural dislocation causing interleaving of quartz-feldspar porphyry and greenstone. The quartz-feldspar porphyry crops out in a zone of intense foliation that coincides with the northeastward projection of the Dome fault.

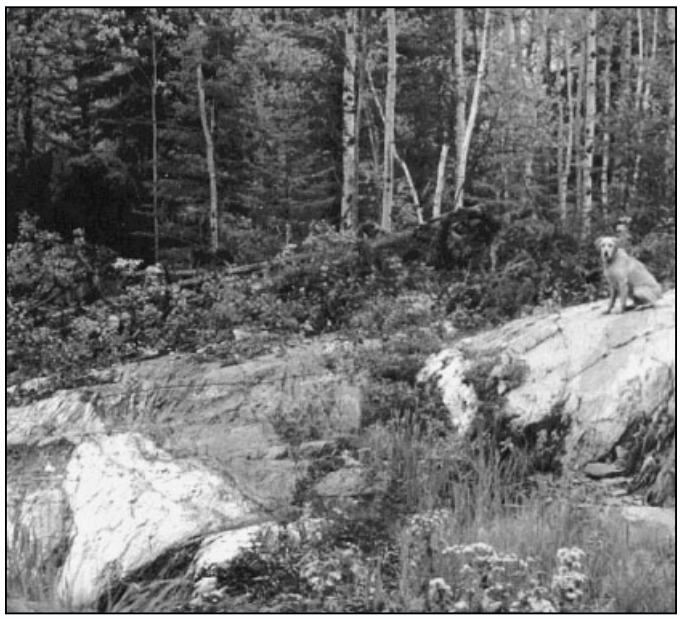

FIG. 9. Photograph of quartz-feldspar porphyry outcrops (white) in greenstone (dark gray) at the Foley O'Brien claim. Photo was taken looking along strike of foliation.

Feldspar porphyry crops out in bodies that, unlike quartz-feldspar porphyry, clearly transect the volcanic strata, indicating that it too intruded the greenstones. In the Blueberry Hill pit, feldspar porphyry is in razor sharp but irregular contact with greenstones. No chilled margins, baking, or xenoliths of country rock were observed along this contact. Surface exposures east of the pit highwall have been covered with waste, but unpublished Dome Mines Ltd. surface maps (M. McCulloch, 1948) show the porphyry to extend 75 m southeastward from the mapped pit exposure (Fig. 7). In the Foley O'Brien claims, feldspar porphyry crops out in a westerly trending, irregular belt, 12 to 35 m wide, which terminates eastward at a fault contact against massive greenstones and westward against the projection of the Dome fault (Fig. 7). Contacts with the host greenstone are discordant and sharp, and no chilled margins or xenoliths of country rock were observed along them. Quartz-feldspar porphyry and feldspar porphyry were nowhere mapped in contact with each other.

U-Pb geochronology

Field relationships plainly show that both quartz-feldspar porphyry and feldspar porphyry are younger than the greenstones and that the former is probably younger than the conglomerates and graywackes at Blueberry Hill. Aitken (1988) described xenoliths of graywacke in porphyry at Blueberry Hill and elsewhere in the Dome property. Evans (1944), Holmes (1968), and Brisbin (1997) described porphyry contacts that cut bedding in the sedimentary strata, and all inferred that the porphyries are younger than these strata, which unconformably overlie Tisdale Group lavas and have been assigned a Timiskaming age (Hurst, 1939; Ferguson, 1968; Holmes, 1968; Brisbin,1997). The field relationships and a new radiometric age date presented in this study support Brisbin's (1997) suggestion that the Timiskaming graywackes and conglomerates at the Dome mine may be older than the Timiskaming strata exposed in the western portion of the district. A sample of quartz-feldspar porphyry collected from the Blueberry Hill pit was selected for geochronological study and a U-Pb zircon date fixes its emplacement at 2688 ± 2 Ma, providing a minimum age for the strata it cuts. Published radiometric age dates of basal Timiskaming strata exposed at the Pamour mine, 12 km east of the Dome mine, indicate that there, the onset of Timiskaming sedimentation was 3 to 15 m.y. later, at 2679 ± 4 Ma (Corfu et al., 1991). The highly variable nature of both the depositional setting of the basal Timiskaming sediments and substrate upon which they lie (Born, 1996) suggests that sedimentation upon the Timiskaming unconformity surface was diachronous, in accordance with the geochronological data of this study.

Distribution of gold and copper

Since 1991, exploration and development have revealed that the Blueberry Hill-Foley O'Brien area is pervasively enriched in Au and Cu. This contrasts with gold concentrations elsewhere at the Dome mine, which are generally tightly restricted to veins or structures and their immediate wall rocks and lack significant Cu. The gold enrichments at Blueberry Hill-Foley O'Brien are associated with both large- and small-scale structural features. A northeast-trending, broad zone of pervasively auriferous and cupriferous rocks at least 60 m wide extends at least 700 m northeast from the Blueberry Hill pit to the abandoned Ontario Northland Railroad tracks. This zone coincides with the extent of the surface exposure of the intrusive quartz-feldspar porphyry and is centered about the Dome fault. Exploration stripping shows that the rocks within the zone are pervasively carbonatized, sericitized, and intensely foliated. Unpublished Placer Dome data (D. Hunt, 1993) show that in the Foley O'Brien claims the minimum gold assay, from 256 1.5-m channel samples from this zone, is 0.10 ppm Au, and the mean is 0.58 ppm . The same samples have an average copper content of 463 ppm. This zone lies within a broader one of lower but still anomalous gold content. At the southwest end of the zone 106,814 t of ore averaging 1.2 ppm Au were mined from the Blueberry Hill pit (E. Kallio, pers. commun., 1993). Data from exploration and blast hole drilling reveal pervasive gold enrichments within an area approximately 100 × 130 m surrounding the pit, and the limits are undefined. An unpublished Placer Dome report (D. Sketchley, 1993) summarizes assay data from 1656 exploration drill core samples representing all exposed rock types in the area of the pit. These have a mean gold content of 1.80 ppm and a median value of 0.47 ppm. Copper assays are available for 625 of these samples and yield a mean Cu content of 0.19 percent Cu. Gold assays form two lognormally distributed populations, and gold and copper contents do not positively correlate (correlation coefficient = 0.14).

Kerrich and Hodder (1982) reported the metal contents of a variety of gold ores from the Dome, Aunor, and McIntyre mines, which show no appreciable copper enrichment in these typical ores of the district, with an average content of only 57 ppm. The same data show that five types of gold ore from the Dome mine, represented by 49 samples, have a weighted average copper content of only 31 ppm, and no single ore type averages more than 70 ppm Cu. Thus, the copper concentrations reported in this study at Blueberry Hill-Foley O'Brien are of particular interest because they are at least 10, and up to 100 times, greater than those of typical gold ores of the district. The Blueberry Hill orebody is, however, geochemically similar to a porphyry-hosted orebody at the McIntyre mine (Davies and Luhta, 1978; Mason and Melnik, 1986b; Melnik-Proud, 1992).

Data from this study (Table 4) show another significant geochemical difference between mineralized quartz-feldspar porphyry at Blueberry Hill-Foley O'Brien and typical ores of the Dome mine, the former having an unusually low Au/Ag ratio compared to the latter. Typical Au/Ag ratios for the Dome mine ores are approximately 6/1 (E. Kallio, pers. commun., 1993), whereas mineralized quartz-feldspar porphyry of this study has a ratio of 0.2/1. Data of Kerrich and Hodder (1982) show an Au/Ag ratio of approximately 10/1 for various types of veins at the Dome mine, with the exception of porphyry-hosted veins which had an average Au/Ag ratio of only 0.3/1. Detailed descriptions of the porphyry-hosted veins and host porphyry were not presented by Kerrich and Hodder (1982), but their data are interesting and relevant in documenting a geochemical contrast between porphyry-related and typical ores similar to that of this study.

Mapping and sampling of the Blueberry Hill pit show that the broad, pervasively copper-gold mineralized zone is cut by

Table 4. Metal Contents (ppm) of Feldspar Porphyry and Quartz-Feldspar Porphyry, Blueberry Hill Area

Sample no.	Rock type	Au	Ag	Cu	Pb	Zn	Mo	As	Sb	Hg
BBH2	QFP	0.238	2.0	1337	4	40	17	18.0	1.6	0.015
BBH3	QFP	0.169	2.3	2528	6	9	22	14.0	1.5	0.018
BBH5	QFP	1.094	1.4	535	5	7	18	22.0	2.0	0.040
BBH7	QFP	0.050	2.9	2968	10	16	18	1.8	0.9	<0.010
BBH10	QFP	0.227	0.9	315	5	10	6	5.7	0.7	<0.010
BBH11	QFP	0.130	1.0	1574	3	7	49	6.5	2.1	0.026
BBH15	QFP	0.321	2.8	3739	3	56	21	7.4	1.6	0.030
BBH16	QFP	0.142	1.6	1314	5	53	13	8.2	1.0	0.013
BBH21	QFP	0.109	0.7	30	<2	8	2	15.0	1.0	<0.010
BBH24	QFP	1.354	3.1	4705	9	16	12	52.0	1.2	0.029
BBH26	QFP	0.162	0.4	352	2	12	3	56.0	2.8	<0.010
BBH52	QFP	0.206	1.6	2481	7	15	29	7.2	0.3	<0.010
FOB10	QFP	0.124	18.0	545	3	64	4	88.0	4.0	0.069
DDH24153 39.5-43	QFP	0.111	1.0	837	101	759	16	7.0	1.4	0.025
DDH24153 87-87.9	QFP	0.402	1.0	3065	7	26	28	25.0	0.9	<0.010
DDH24153 71-72.5	QFP	0.112	0.7	1250	4	36	24	14.0	0.4	<0.010
DDH24153 133-134.5	QFP	0.261	0.3	774	4	16	17	4.1	0.5	<0.010
DDH24153 146-147	QFP	0.137	<0.2	160	<2	28	15	15.0	0.3	<0.010
DDH24153 170-171	QFP	0.242	0.8	846	3	29	14	14.0	0.5	<0.010
DDH24154 16-17.5	QFP	0.102	0.9	22	8	107	2	12.0	1.2	<0.010
DDH24155 320.5-321.5	QFP	0.067	0.6	647	3	24	11	11.0	<0.2	<0.010
DDH24155 325-326	QFP	0.185	0.6	46	5	23	16	22.0	<0.2	<0.010
DDH24156 16-17	QFP	0.537	0.6	474	3	9	8	50.0	1.3	<0.010
DDH24156 21-22.4	QFP	0.237	<0.2	13	3	13	2	8.3	0.6	<0.010
DDH24157 87.25-88.5	QFP	0.456	0.4	96	20	653	3	30.0	0.7	0.027
DDH24157 138.8-139.9	QFP	0.144	2.3	1202	5	124	4	4.8	1.1	<0.010
DDH24157 179.3-179.9	QFP	0.100	0.7	211	3	33	2	6.6	0.7	<0.010
DDH24157 184.6-186	QFP	0.031	0.2	58	3	16	3	1.0	0.2	<0.010
DDH24159 22.8-23.55	QFP	0.085	3.4	22	4	11	2	15.0	0.8	0.011
DDH24159 37.9-38.9	QFP	1.040	0.5	171	<2	13	4	39.0	0.6	<0.010
DDH24159 257.5-259	QFP	0.858	0.6	346	3	26	5	46.0	0.5	<0.010
DDH24159 289.8-290.8	QFP	0.158	0.8	1328	3	12	75	17.0	<0.2	<0.010
DDH24161 44-45.5	QFP	0.370	1.3	1163	13	16	11	61.0	2.5	0.042
DDH24161 64.5-66	QFP	0.184	<0.2	11	3	9	140	36.0	1.2	<0.010
H2733	QFP	0.173								
H2734	QFP	0.491								
H2736	QFP	0.435								
H2750	QFP	0.115								
H2752	QFP	0.040								
H2770	QFP	0.025								
H2808	QFP	0.124								
H2833	QFP	0.383								
Average		0.284	1.8	1034	8	68	18	21.8	1.1	0.017
Standard deviation		0.298	3.0	1185	17	165	26	20.4	0.8	0.013
FOB1	FP	<0.005	1.2	105	<2	25	<1	31.0	0.8	<0.010
FOB2	FP	<0.005	0.5	4	<2	15	<1	4.3	0.8	<0.010
FOB3	FP	<0.005	0.5	8	9	60	<1	6.1	<0.2	0.188
FOB4	FP	<0.005	0.5	38	<2	26	<1	20.0	<0.2	<0.010
FOB5	FP	<0.005	1.1	5	<2	23	<1	7.9	1.9	<0.010
FOB6	FP	<0.005	0.3	12	<2	17	<1	23.0	1.3	<0.010
FOB7	FP	<0.005	3.3	20	<2	22	<1	41.5	3.1	<0.010
FOB8	FP	<0.005	20.0	52	<2	19	<1	11.0	2.4	<0.010
FOB9	FP	<0.005	1.6	96	<2	18	<1	14.0	1.3	0.014
BBH37	FP	<0.005	4.5	12	4	17	<1	6.3	<0.2	<0.010
BBH38	FP	<0.005	0.3	8	4	20	<1	6.2	0.3	<0.010
BBH62	FP	<0.005	0.1	5	11	15	<1	7.4	0.2	0.007
BBH65	FP	<0.005	0.1	6	5	19	<1	3.2	3.5	0.009
H2764	FP	0.04								
H2772	FP	<0.005								
H2792	FP	<0.005								
H2804	FP	<0.005								
H2806	FP	<0.005								
H2818	FP	<0.005								
H2819	FP	<0.005								
Average		0.007	2.6	28	4	23	<1	14.0	1.2	0.024
Standard deviation		0.008	5.4	35	3	12	<1	11.7	1.2	0.049

Abbreviations: QFP = quartz-feldspar porphyry, FP = feldspar porphyry
Note: Analyses less than detection limit set to detection limit for calculation of means and standard deviations

discrete auriferous fault zones and various types of auriferous veins. These crosscutting auriferous features include (1) east-northeast–striking, southeast-dipping quartz veins and west-northwest–striking, south-dipping quartz veins, hosted by all rock types, which contain coarse visible Au; (2) subhorizontal, stacked, curvilinear quartz + sulfide veins hosted by greenstone which assayed up to 7.85 ppm Au; (3) northeast-striking, subvertical, joint-controlled stringers and lenses of pyrite-tourmaline, 0.01 to 20 cm thick, hosted only by quartz-feldspar porphyry, which assayed up to 2.89 ppm Au; (4) northeast-striking, subvertical, joint-controlled lenses of pyrite + chlorite + chalcopyrite, 2 to 40 cm thick, hosted only by quartz-feldspar porphyry, which contain up to 2.95 ppm Au; and (5) north-, northwest-, and northeast-striking fault and gouge zones that transect all rock types and contain up to 2.88 ppm Au.

Geochemical comparison of porphyries

Geochemical studies of the two felsic porphyries reveal striking contrasts between their gold contents. Table 4 shows that quartz-feldspar porphyry is ubiquitously gold enriched, whereas feldspar porphyry is uniformly gold barren. Gold assays for 42 quartz-feldspar porphyry samples average 0.28 ppm, every sample containing detectable Au, the minimum value being 0.03 ppm. Gold content, moreover, is relatively uniform, 31 of 42 samples containing between 0.10 and 0.50 ppm; only 6 of 42 samples less than 0.10 ppm Au, and only 5 of 42 more than 0.50 ppm. This result was unexpected, because during sampling care was taken to collect many apparently unmineralized samples, as well as apparently mineralized ones. The latter contained megascopically discernible quartz veining or abundant sulfide, whereas the former lacked these features.

In sharp contrast to the data for quartz-feldspar porphyry samples, samples of feldspar porphyry were uniformly barren of Au. The average gold assay for 20 samples of feldspar porphyry is less than 0.007 ppm, and this average is strongly influenced positively by a single sample that assayed 0.04 ppm. None of the remaining 19 samples contained Au above a 0.005 ppm detection limit. Production blast hole data from the Blueberry Hill pit confirm the gold-poor nature of feldspar porphyry. Geologic data are not available for the individual 6-m deep blast holes but significantly, composite assay data show that only 22 of 1,000 production blast holes averaged less than the assay detection limit of 0.004 oz/t (0.14 ppm Au), and 18 of these 22 gold-barren holes were drilled along the north-northwest projection of the dike of feldspar porphyry exposed in the pit high wall (Fig. 7). A significant finding of this study, therefore, is that feldspar porphyry is the only rock in the Blueberry Hill-Foley O'Brien area that does not contain detectable Au above the 0.005 ppm detection limit.

Other striking geochemical differences between the two porphyries are evident in Table 4. Multielement geochemical data show that elevated Cu and anomalous Mo contents accompany Au in quartz-feldspar porphyry. Ubiquitously auriferous quartz-feldspar porphyry averages 1,034 ppm Cu and 18 ppm Mo (Table 4), which contrasts strongly with gold-barren feldspar porphyry which averages 28 ppm Cu and <1 ppm Mo. The very low Cu content of feldspar porphyry is also striking because the entire Blueberry Hill-Foley O'Brien area is anomalously copper enriched. The geochemical contrast between the copper-barren feldspar porphyry and its host rocks is particularly marked within the Blueberry Hill Au-(Cu) orebody. The orebody averages 0.19 percent Cu yet samples of the feldspar porphyry dike that cuts it average only 8 ppm Cu, with a maximum of 12 ppm.

Interpretation of Absolute and Relative Timing of Gold Deposition

Data from this study indicate that at least three broad episodes of gold deposition affected the Porcupine camp: (1) an early period that occurred prior to development of the Timiskaming unconformity surface, (2) an epigenetic Cu-Au-Mo event that was contemporaneous with felsic magmatic activity, and (3) an economically important gold vein-forming event that postdates felsic magmatic activity, porphyry emplacement, and Timiskaming sedimentation. The pre-Timiskaming event is manifested by auriferous clasts in the basal Pamour conglomerate. Although the source of the clasts cannot be conclusively determined, they are clearly shown to be derived from preexisting auriferous deposits and are compelling evidence of gold mineralizing events that predate development of the Timiskaming unconformity surface. The pyritic clasts in particular, with an average content of 2.54 ppm Au, are evidence for a pre-Timiskaming period of significant gold concentration in auriferous pyritic deposits. If these clasts were derived from interflow sedimentary rocks of the Tisdale Group, or from iron-formation of the Deloro Group, they are evidence for early, synsedimentary gold deposition. If they were derived from a different source, they represent a pre-Timiskaming gold depositional event of unknown nature. The banded sulfidic quartz clasts closely resemble iron-formation of the Deloro Group, and such a parentage is here suggested. The sulfidic quartz clasts, which resemble ore from auriferous veins in the district, suggest a pre-Timiskaming, but epigenetic gold vein-forming event possibly related to early magmatic activity evidenced by intrusions emplaced into the Deloro Group strata or by Tisdale Group felsic volcanism. Ultramafic, monzonitic, and granodioritic plutons invade rocks of the Deloro Group but not the Tisdale Group, indicating early pre-Tisdale magmatism that could have driven epigenetic vein formation, and quartz veined clasts in Tisdale Group fragmental volcanic strata (Brisbin, 1997) are evidence for epigenetic vein formation associated with felsic volcanism. U-Pb zircon age dates of detrital zircons (Corfu at al., 1991) indicate that deposition of the Pamour conglomerate began at or after 2679 ± 4 Ma and provide an approximate minimum age of formation of the source rock for the gold mineralized clasts.

Two epigenetic gold-depositing events that postdate development of the Timiskaming erosional surface at the Dome mine are distinguished based on their temporal associations with a period of felsic magmatic activity. Early Cu-Au-Mo deposition is closely linked in time to emplacement of felsic porphyries, and economically important gold vein generation postdates felsic porphyry emplacement. Based on petrologic, rare earth elemental, and immobile oxide geochemical studies, previous workers have interpreted that the felsic porphyritic stocks and dikes in the Timmins district are comagmatic

(Griffis, 1968; McAuley, 1983; Burrows and Spooner, 1986, 1989). The two types of porphyritic intrusions documented in this study are petrologically similar, both to each other and to other felsic porphyries in the district. Major oxide geochemical data from this study (App. 2) combined with data of Ferguson (1968) show that the former are also chemically similar to the other porphyries of the district. Unpublished rare earth elemental data and chondrite normalized diagrams prepared for Placer Dome (J. Gardiner, 1991) also show that mineralized quartz-feldspar porphyry from Blueberry Hill is indistinguishable from the Paymaster, Preston, West Preston, Coniaurum, Pearl Lake, Miller Lake, Crown, Edwards, and Gillies Lake porphyries. U-Pb zircon age dating of five porphyritic stocks in the district yields ages ranging from 2688 to 2691 Ma (Corfu et al., 1989). The age date for quartz-feldspar porphyry presented in this study, 2688 ± 2 Ma, is identical to that of the other porphyries in the district. For these reasons, quartz-feldspar porphyry and feldspar porphyry are interpreted to be comagmatic with the other felsic porphyries of the district.

The significant finding of this study that feldspar porphyry is the only unmineralized rock in the Blueberry Hill area, although it discordantly intrudes a zone of pervasive Cu-Au-(Mo) mineralization centered upon, and partly hosted by well-mineralized quartz-feldspar porphyry, is relevant to dating mineralizing events. The discordant feldspar porphyry is conspicuously lacking in copper and gold enrichments compared to its immediate wall rock and significantly, although both quartz-feldspar porphyry and feldspar porphyry have been sericitized, carbonatized, and pyritized to similar degrees, chalcopyrite-bearing veinlets and lenses that are common in quartz-feldspar porphyry are absent in feldspar porphyry, and the disseminated chalcopyrite that is ubiquitous to quartz-feldspar porphyry is uncommon in feldspar porphyry. Quartz-feldspar porphyry and feldspar porphyry are chemically and petrologically similar, thus it seems doubtful that chemical or rheological contrasts between the lithologies would result in such marked contrasts in metal contents, sulfide mineralogy, and veinlet formation. These contrasts are best explained by ascribing an age to the feldspar porphyry intrusion that postdates formation of the chalcopyrite-bearing veinlets and the Cu-Au-(Mo) mineralizing event. In this case, the latter is bracketed in time by the earlier intrusion of quartz-feldspar porphyry and the later intrusion of the younger but comagmatic feldspar porphyry, and a close temporal relationship between Cu-Au-(Mo) mineralization and quartz-feldspar porphyry felsic intrusive activity is indicated. An age of 2688 ± 2 Ma is therefore inferred for quartz-feldspar porphyry magmatism and Cu-Au-(Mo) mineralization. This porphyry-related Cu-Au-(Mo) mineralization, however, forms less than one-half of one percent of the mineable gold resource at the Dome mine.

Discordant field relationships clearly show that most gold deposition postdates emplacement of felsic porphyries at the Dome mine. At Blueberry Hill, planar and sheeted auriferous quartz veins cut early, pervasive, quartz-feldspar porphyry-hosted Cu-Au-(Mo) mineralization, transect foliation (Fig. 10), and crosscut, and hence postdate, chalcopyrite-bearing veinlets and lenses. Similar auriferous quartz veins transect barren feldspar porphyry that itself cuts the early Cu-Au-(Mo) mineralized zone. Visible Au, including coarse clusters of grains containing several grams, was observed in these veins, and they are spatially associated with zones of pervasive carbonatization and sericitization that extend beyond the limits of economic mineralization and affect greenstone and both types of porphyry. Similar ore alteration relationships are true of gold deposits throughout the district (Ferguson, 1968; Griffis, 1968; Holmes, 1968; Jones, 1968; Aitken, 1990) and the auriferous Blueberry Hill quartz veins are similar to the vein systems which have yielded most of the gold ore at the Dome mine and both are interpreted to have formed during the same event, i.e., subsequent to emplacement of both porphyries. Additional evidence of this is in the 3 shaft area open pit and in underground workings, where auriferous quartz veins transect felsic porphyry. Just as at Blueberry Hill, some undeformed planar and sheeted veins and some en echelon veins, often containing coarse Au, cut across foliation. Because the porphyry is itself foliated yet is cut by some undeformed auriferous quartz veins, a period of deformational fabric development must postdate porphyry emplacement but predate formation of the undeformed auriferous veins. A significant time gap of unknown duration between emplacement of porphyry and formation of the later auriferous veins is implied. Identical relationships and conclusions regarding porphyry emplacement, deformation, and formation of auriferous veins have been documented at the Hollinger and McIntyre mines (Wood et al., 1986; Burrows et al., 1993), and

FIG. 10. Photograph taken looking southeast at northwest-striking, southwest-dipping, planar, sheeted, auriferous quartz veins cutting foliated quartz-feldspar porphyry in Blueberry Hill pit. Schistosity in quartz-feldspar porphyry is multidirectional, with dominant foliation striking northeast and dipping southwest, to left in photo.

geochronological studies (Corfu et al., 1989) indicate that emplacement of porphyry and auriferous vein formation was separated by at least 9 m.y. However, Mason and Melnik (1986b), and Melnik-Proud (1992) described auriferous veins and orebodies at McIntyre that share the same penetrative deformation fabric as their host rocks, therefore concluding that gold mineralization predated development of deformation fabrics. An albitite dike that is cut by auriferous veins at McIntyre has been dated at 2673^{+6}_{-2} Ma (Corfu et al., 1989), providing a maximum age for the latest gold deposition in the camp.

Discussion

The ores of the Porcupine camp are representative of a broad class of Archean lode gold deposits. Features common to such deposits (Hutchinson, 1993; Robert and Poulsen, 1997) include: Archean age of host rocks and mineralization; host greenstone terranes that include ultramafic to felsic volcanic rocks, their subvolcanic and/or plutonic equivalents, and clastic and chemical sedimentary rocks; association with major structural zones; great vertical extent (1–2 km) of mineralization, commonly lacking appreciable mineralogical and/or geochemical zoning; associated carbonate alteration at both deposit and district scale; nonspecificity of host rocks within the greenstone terrane; common spatial association with felsic intrusive rocks; common occurrence at or near a volcanic-sedimentary rock interface; and ores of both stratiform and markedly discordant (vein) morphology, the latter clearly introduced late in tectonic evolution of the host terrane. Data from this study and others (Moore, 1977; Bavinton and Keays, 1978; Boyle, 1979; Saager et al., 1982; Downes et al., 1984; Gross, 1988) suggest that early gold enrichments into supracrustal rocks may be another feature common to these deposits. The documentation here of multiple stages of gold emplacement, over at least 7 m.y., into a productive greenstone terrane is important in relation to genetic hypotheses for the ores and may also be significant in exploration for Au in other Archean greenstone districts.

In the Porcupine camp, the existence of early gold concentrations, some ore grade, is unequivocally demonstrated by the presence of strongly auriferous clasts in the Timiskaming conglomerate. If such early gold enrichments are widespread throughout the greenstone belt, an untested hypothesis, then a significant amount of gold-enriched rock may have been available to interact with later metamorpho- or magmatogenic hydrothermal fluids, to serve as protore to the lode deposits. Moreover, early syndepositional pyrite in iron-formation or carbonaceous argillite would provide a readily available source of sulfur. At greenschist facies temperatures, breakdown of pyrite to pyrrhotite would liberate sulfur to form sulfide and/or bisulfide complexes which, in turn, could transport Au remobilized from the same source rocks. Although some workers believed that a gold-enriched protore was not a prerequisite to ore genesis (Boyle, 1979; Anhaeusser, 1981; Colvine, 1989), primary, premetamorphic differences in gold abundance may help to explain why seemingly similar greenstone terranes have remarkably different productive histories. This issue is of both academic interest and practical importance to explorationists and economic geologists alike. The heterogeneous gold productivity of greenstone belts is exemplified in the Archean Superior province of Canada, where 85 percent of gold production and reserves are creditable to one of many greenstone belts, the Abitibi (Card et al., 1989). Although the huge extent of the Abitibi belt may in part account for this, one wonders too why some smaller greenstone belts, like Red Lake in northwestern Ontario, are important producers whereas other small but similar belts are not. Similar relationships have been discussed for the Archean Yilgarn block in Western Australia (Groves et al., 1987). Although extrapolation of results from a single study of a specific district to deposits worldwide is hazardous, it is interesting that in one of the world's most productive Archean lode gold districts, the Porcupine camp, multiple stages of gold introduction into supracrustal rocks occurred prior to later economically important vein ore formation. It would be instructive to study both productive and economically barren greenstone terranes by comparing both cyclicity of gold deposition and nature and extent of premetamorphic gold enrichments to extent of ore formation. Perhaps repeated introduction and/or remobilization of Au were necessary to form the most productive districts, or alternatively, perhaps repeated introductions of Au define an inherently gold-rich greenstone belt, with no direct genetic link between early and late gold deposition. In either case, recognition of multicyclic gold deposition becomes an empirical discriminant between potentially productive belts and those that may host only small, economically unimportant deposits that typify most greenstone terranes.

The timing and nature of porphyry emplacement, and its genetic relationship to gold deposits in the Porcupine camp, is of particular interest because of the spatial association of many important gold deposits with porphyritic stocks. Through 1999, 49,865,767 oz of Au, comprising 79 percent of the total recorded district production of ~62,800,000 oz (government and published company production records), has come from orebodies located mainly adjacent to, but sometimes within, felsic porphyritic rocks, including orebodies of the Hollinger, McIntyre, Coniaurum, Dome, Paymaster, and Preston mines (Fig. 1). The genetic relationship between the felsic porphyries and gold deposits has long been highly contentious. Most investigators concluded that ores of the district significantly postdate felsic intrusive activity (Wood et al., 1986; Marmont and Corfu, 1989; Burrows et al. 1993), and this has been interpreted more broadly as applicable to Archean lode gold deposits of the Superior province in general (Corfu, 1993). Wood et al. (1986), Burrows and Spooner (1986), and Burrows et al. (1993) considered that links between felsic porphyries and gold ore formation were passive and purely structural. Mason and Melnik (1986a, b) concluded that some ores of the district were formed by porphyry-type hydrothermal systems but the exposed porphyries were not the causative intrusions. Melnik-Proud (1992) and Brisbin (1997) linked mineralization to hydrothermal activity related to emplacement of albitite dikes, which preferentially intrude felsic porphyries.

Most evidence regarding possible genetic relationships between felsic intrusive activity and gold deposition derives from studies of the Hollinger and McIntyre mines. The latter hosted an atypical orebody that yielded 175,000 oz of Au from 10 Mt of porphyry-hosted ore with an average recovered

grade of 0.67 percent Cu, 0.6 ppm Au, 2.9 ppm Ag, and unrecovered Mo at 0.05 percent (Burrows and Spooner, 1986). This enigmatic Cu-Au-(Mo) orebody was superimposed upon a breccia pipe within the Pearl Lake Porphyry, about which zones of albititic and hematitic-anhydritic alteration were developed. For proper perspective, however, it is important to note that the Hollinger-McIntyre deposits also produced in excess of 30 Moz of Au from quartz-carbonate lodes and vein systems that are typical of ores of the district as a whole. These occurred primarily around the margins of the Pearl Lake Porphyry, hosted in greenstones of the Tisdale Group. This atypical Cu-Au-(Mo) deposit has generally been distinguished from the gold ores (Ferguson, 1968; Kerrich and Hodder, 1982; Pyke, 1982; Burrows and Spooner, 1986), but Melnik-Proud (1992) and Mason and Melnik (1986a, b) believed that the two were, in fact, intimately related. They concluded that the Hollinger-McIntyre deposits, both Cu-Au-(Mo) and Au-only, formed in a gold-dominated, near-surface, porphyry-type hydrothermal system, with porphyry copper stockwork mineralization surrounded by a peripheral zone of gold veins. Burrows et al. (1993) argued that these gold veins formed as an integral part of shear zone development and were not related to a porphyry system.

Important findings from this study may help reconcile some aspects of these contradictory interpretations regarding genetic relationships of felsic intrusions to gold mineralization. Our observations and interpretations at the Blueberry Hill-Foley O'Brien deposits bear on this problem and may be applicable, to some extent at least, to other important deposits of the district, particularly the Dome and McIntyre deposits. They include: (1) some Au was deposited with Cu-Au-(Mo) mineralization, which is closely associated temporally with quartz-feldspar porphyry emplacement; (2) many, probably most of the rich gold veins, significantly postdate porphyry emplacement; and (3) various characteristics of orebodies and mineralized rock, as presently observed, formed through superposition of multiple mineralizing events.

Evidence that mineralization at Hollinger-McIntyre is associated with a large porphyry-type hydrothermal system comes from study of the atypical Cu-Au-(Mo) orebody at the McIntyre mine (Mason and Melnik, 1986a, b; Melnik-Proud, 1992). This orebody is similar to the mineralization exposed near the 8 shaft in the Blueberry Hill pit at the Dome mine. When compared to ores of the district as a whole, both are atypically enriched in Cu and Mo, relatively low in Au relative to Ag, and intimately associated with a felsic porphyritic intrusion. Discordant field relationships at Blueberry Hill-Foley O'Brien and data of this study suggest that the Cu-Au-(Mo) mineralization there is temporally associated with felsic intrusive activity and predates geochemically and morphologically different, and much more economically significant, gold vein formation. If analogously, the Cu-Au-(Mo) mineralization at McIntyre formed nearly contemporaneously with emplacement of felsic intrusions (albitite dikes or the older Pearl Lake Porphyry) and was subsequently affected by a younger, gold vein-forming event, then the contradictory interpretations regarding timing of gold deposition, deformation, and genetic significance of the felsic porphyries arise from failure to distinguish superimposed mineralizing events. Recent genetic interpretations for the Hollinger-McIntyre orebodies (Mason and Melnik, 1986a, b; Wood et al., 1986; Melnik-Proud, 1992; Burrows et al., 1993) and, by extension, many ores of the district (Brisbin, 1997) are predicated upon a single mineralizing event and do not adequately explain all the complex and varied field and geochemical characteristics of the deposits. A hypothesis that recognizes a Cu-Au-(Mo) mineralizing event related to felsic intrusions and a later gold vein-forming event best explains these characteristics.

The marked differences in timing, field relationships, and geochemical signatures between the progenitor sources of the gold-mineralized clasts, the atypical, porphyry-affiliated Cu-Au-(Mo) deposits, and the typical late, gold-rich veins are significant to current contradictory understandings of ore genesis in the Timmins district. The differences strongly indicate that different and sequential hydrothermal systems formed these differing gold deposits. Gold enrichment that predated formation of the Timiskaming unconformity surface is manifested by auriferous clasts in the basal conglomerate. These lack the Cu-Au-(Mo) association of the porphyry-affiliated ores. The latter have a distinct mineralogic and minor element signature, closely resembling that of Phanerozoic porphyry-copper deposits (Davies and Luhta, 1978). This suggests magmatogenic, porphyry-related, high-temperature and Cl-dominated hydrothermal activity, which introduced a suite of metals very different from that of both the pre-Timiskaming gold-dominated deposits and later veins. This magmatogenic system may have assimilated some of its Au from older auriferous strata, which it overprinted. The later, economically important vein systems may themselves belong to different sets of different ages, but in any case they clearly postdate both earlier types of deposits. They lack the distinctive Cu-Au-(Mo) signature of the porphyry-affiliated deposits. This suggests a younger, reduced complex-dominant, lower temperature hydrothermal system, perhaps generated during regional metamorphism that affected all rocks of the district. Whatever their specific nature and derivation, this study clearly indicates that during at least 7 m.y., and perhaps as much as 19 m.y., at least three successive and distinct mineralizing epochs were involved in forming the various gold deposits of the Timmins district and that products of the later ones were superimposed on those of the earlier ones. The latest hydrothermal gold mineralizing epoch was clearly the most important economically and formed most of the exploited ores. At least two of the three gold-emplacing events documented in this study predate regional metamorphism, thus are permissive and supportive of genetic hypotheses that invoke metamorphogenic remobilization of Au from earlier formed deposits.

The sequencing of gold-depositing events indicated by this study is simplified and incomplete, elucidating relationships between some, but not all, gold deposit types in the Porcupine camp. Further studies are required for a full understanding of gold deposition throughout the camp. If auriferous clasts in basal Timiskaming conglomerate were not derived from Deloro Group iron-formation or Tisdale Group interflow sedimentary strata, then additional gold-depositing events of unknown affinity, predating development of the Timiskaming unconformity are indicated. Further field and analytic studies are needed to constrain the relative and absolute timing of other ore types in the district. In particular,

at the Dome mine the timing of ankerite vein generation relative to development of the Timiskaming unconformity surface and felsic intrusive activity is unknown. The timing of formation of greenstone-hosted, en echelon vein systems and sedimentary rock-hosted stockworks too, is poorly constrained by field relationships, although their structural and geochemical similarities to lodes that crosscut the porphyries suggest that they formed contemporaneously with the latter, thus postdate felsic intrusive activity.

Conclusions

Gold was deposited in supracrustal rocks of the Porcupine camp in distinct, multiple, and successive stages spanning a time period of at least 7 m.y. Three specific stages of gold emplacement are recognized. Auriferous clasts in the basal Timiskaming conglomerate, clearly derived from the older, underlying rocks, prove the existence of pre-Timiskaming gold concentrations. Pyritic clasts contain on average 2.54 ppm Au and are conclusive evidence for the existence of pre-Timiskaming pyritic gold deposits. These clasts may have been derived from pyritic bodies in carbonaceous argillites of the Tisdale Group, from sulfide facies iron-formation of the Deloro Group, or from pyritic massive sulfide deposits of unknown location and genesis. Auriferous banded sulfidic quartz clasts were probably derived from iron-formation of the Deloro Group and auriferous sulfidic quartz clasts perhaps from early epigenetic quartz-sulfide veins.

Two differing types of epigenetic gold deposition are recognized at the Dome mine. Copper, gold, and minor molybdenum were deposited during an event that accompanied emplacement of felsic porphyritic intrusions. These intrusions and the mineralization are clearly cut and overprinted by later planar, sheeted, and en echelon auriferous quartz veins, and by mineralized shear and/or fault zones. Discordant and crosscutting field relationships and differing textures and mineral composition of these veins further indicate multiple stages of vein formation but all postdate emplacement of the felsic porphyritic intrusions.

U-Pb zircon age dates of detrital zircons from Timiskaming sandstone published by Corfu et al.(1991) indicate a maximum age of 2679 ± 4 Ma for the Pamour conglomerate and provide an approximate minimum age for formation of the source rock of the mineralized clasts. Isotopic age dates for mineralized porphyry from this study indicate a 2688 ± 2 Ma age for the Cu-Au-(Mo) mineralizing event. A maximum age for latest gold deposition in the camp is that of an albitite dike, dated at 2673^{+6}_{-2} Ma (Corfu et al., 1989), that is cut by auriferous veins at the McIntyre mine. Thus, multiple periods of Au emplacement into supracrustal rocks, associated with distinctly different geologic events, and occurring over at least 7 m.y., and possibly as much as 19 m.y., are indicated. The post-porphyry veins account for most production from the Dome mine and were formed by hydrothermal activity that significantly postdated emplacement of the porphyries. Although some Au, as well as Cu and minor Mo, was deposited by hydrothermal activity that accompanied emplacement of felsic porphyries, data of this study support earlier interpretations that the porphyries played a passive structural role in localizing the most important ore deposits. The documentation of at least three broad periods of gold emplacement, at least two of which are premetamorphic, is permissive and supportive of genetic hypotheses that invoke metamorphogenic remobilization of Au from earlier formed deposits. Alternatively, the coincidence of early gold enrichments and later richer concentrations may simply reflect an inherently gold-rich terrane in which hydrothermal events tapped the same gold reservoir at different times, forming different types of enrichments and deposits. In either case, the evidence here presented rules out hypotheses that explain all gold deposition in these districts as products of a single, short-lived, syn- or postmetamorphic and epigenetic process, whether by magmatogenic or metamorphogenic hydrothermal fluids. Such hypotheses may indeed explain some, perhaps many late auriferous veins, but fail to account for the earlier, pre-Timiskaming gold enrichments here documented.

Acknowledgments

The authors sincerely thank the many individuals and organizations whose support made this research possible and enjoyable. Placer Dome Inc. provided generous financial and logistical support, and special thanks go to E. Gonzalez-Urien. Access to data, drill core, and property, as well as logistical support was provided by J. Morganti, E. Kimura, T. Lewis, P. Burchell, F. Stewart, J. Gardiner, and the staff of the Placer Dome Timmins Exploration office; E. Kallio and colleagues at the Dome mine; K. Tyler and staff at the Pamour 1 and Hoyle 1 mines; J. Houle, M. Robb, and staff at Royal Oak Mines Inc.; R. Labine of Falconbridge Gold; D. Duff of Falconbridge Exploration; and P. Sangster and the Ontario Geological Survey. J. Warme, G. Holden, R. Eggert, and D. Dickinson provided helpful reviews and discussions. E. van Hees assisted with advice and logistical support, and Q. Hennigh shared his thoughts and lab expertise. *Economic Geology* reviewers François Robert and Dan Brisbin are thanked for improving the manuscript with thoughtful criticisms.

May 24, 1996; December 11, 2000

REFERENCES

Aitken, S.A., 1988, Surface geology adjacent to the no. 8 shaft, Dome Mines Ltd., Tisdale township, Ontario: Unpublished B.Sc. thesis, Kingston, Ontario, Queens University, 39 p.

——1990, The Pamour one mine—site investigation, Timmins, Ontario: Unpublished M.Sc. thesis, Kingston, Ontario, Queens University, 194 p.

Anhaeusser, C.R., 1981, The relation of mineral deposits to early crustal evolution: Economic Geology Seventy-Fifth Anniversary Volume, p. 42–63.

Ayer, J.A., Trowell, N.F., Amelin, Y., and Corfu, F., 1999, Geologic compilation of the Abitibi greenstone belt in Ontario, toward a revised stratigraphy based on compilation and new geochronological results: Summary of filed work and other activities 1998, Ontario Geological Survey Miscellaneous Paper 169, p. 14–24.

Backman, O.L., 1948, Broulan mne, *in* Wilson, M.E., ed., Structural geology of Canadian ore deposits: Montreal, Quebec, Canadian Institute of Mining and Metallurgy Symposium, Jubilee Volume, p. 554–558.

Bavinton, O.A., and Keays, R.R., 1978, Precious metal values from interflow sedimentary rocks from the komatiite sequence at Kambalda, Western Australia: Geochimica et Cosmochimica Acta, v. 42, p. 1151–1163.

Bell, A.M., 1948, Hallnor mine, *in* Wilson, M.E., ed., Structural geology of Canadian ore deposits: Montreal, Quebec, Canadian Institute of Mining and Metallurgy Symposium, Jubilee Volume, p. 547–553.

Born, P., 1996, A sedimentary basin analysis of the Abitibi greenstone belt in the Timmins area, northern Ontario, Canada: Unpublished Ph.D. thesis, Ottawa, Ontario, Canada, Carleton University, 489 p.

Boyle, R.W., 1979, The geochemistry of gold and its deposits: Geological Survey of Canada Bulletin 280, 584 p.

Brisbin, D.I., 1986, Geology of the Owl Creek and Hoyle Pond gold mines, Hoyle township, Ontario: Unpublished investigative report, Kingston, Ontario, Canada, Queens University, 48 p.
——1997, Geologic setting of gold deposits in the Porcupine mining district, Timmins, Ontario: Unpublished Ph.D. thesis, Kingston, Ontario, Canada, Queens University, 523 p.
Buffam, B.S., 1968, Description of properties, Moneta Porcupine Mines Limited: Ontario Department of Mines Geological Report 58, p. 134–138.
Burrows, A.G., 1911, The Porcupine gold area: Ontario Bureau of Mines, v. 20, pt. 2, p. 1–39.
——1912, The Porcupine gold area, second report: Ontario Bureau of Mines, v. 21, pt. 1, p. 205–249.
——1915, The Porcupine gold area, third report: Ontario Bureau of Mines, v. 24, pt. 3, p. 1–57.
——1924, The Porcupine gold area, fourth report: Ontario Department of Mines, v. 33, pt. 2, 112 p.
Burrows, D.R., and Spooner, E.T.C., 1986, The McIntyre Cu-Au deposit, Timmins, Ontario, Canada, *in* Macdonald, A.J., ed., Gold '86: Willowdale, Ontario, Konsult International, p. 23–39.
——1989, Relationships between Archean gold quartz vein-shear zone mineralization and igneous intrusions in the Val d'Or and Timmins areas, Abitibi subprovince, Canada: Economic Geology Monograph 6, p. 424–444.
Burrows, D.R., Spooner, E.T.C., Wood, P.C., and Jemielita, R.A., 1993, Structural controls on formation of the Hollinger-McIntyre Au quartz vein system in the Hollinger shear zone, Timmins, southern Abitibi greenstone belt, Ontario: Economic Geology, v. 88, p. 1643–1663.
Card, K.D., Poulsen, K.H., and Robert, F., 1989, The Archean Superior province of the Canadian Shield and its lode gold deposits: Economic Geology Monograph 6, p. 19–36.
Carter, O.F., 1968, Description of properties, Westfield Minerals Limited (Coniaurum): Ontario Department of Mines Geological Report 58, p. 153–158.
Colvine, A.C., 1989, An empirical model for the formation of Archean gold deposits: Products of final cratonization of the Superior province, Canada: Economic Geology Monograph 6, p. 37–53.
Corfu, F., 1993, The evolution of the southern Abitibi greenstone belt in light of precise U-Pb geochronology: Economic Geology, v. 88, p. 1323–1340.
Corfu, F., Krogh, T.E., Kwok, Y.Y., and Jensen, L.S., 1989, U-Pb zircon geochronology in the southwestern Abitibi greenstone belt, Superior province: Canadian Journal of Earth Sciences, v. 26, p. 1747–1763.
Corfu, F., Jackson, S.L., and Sutcliffe, R.H., 1991, U-Pb ages and tectonic significance of late alkalic magmatism and non-marine sedimentation: Timiskaming Group, southern Abitibi belt, Ontario: Canadian Journal of Earth Sciences, v. 28, p. 489–503.
Davies, J.F., 1977, Structural interpretation of the Timmins area, Ontario: Canadian Journal of Earth Sciences, v. 14, p. 1046–1053.
Davies, J.F., and Luhta, L.E., 1978, An Archean "porphyry-type" disseminated copper deposit, Timmins, Ontario: Economic Geology, v. 73, p. 383–396.
Davies, J.F., and Whitehead, R.E.S., 1980, Further immobile element data from altered volcanic rocks, Timmins mining area: Canadian Journal of Earth Sciences, v. 17, p. 419–423.
Downes, M.J., Hodges, D.J., and Derweduwen, J., 1984, A free carbon- and carbonate-bearing alteration zone associated with the Hoyle Pond gold occurrence, Ontario, Canada, *in* Foster, R.P., ed., Gold '82: Rotterdam, A. A. Balkema, p. 435–448.
Duff, D., 1982, The petrology and geochemistry of rocks associated with gold deposits, Timmins area, Ontario, Canada: Unpublished M.Sc. thesis, Sudbury, Ontario, Laurentian University, 145 p.
Dunbar, R.D., 1948, Structural relations of the Porcupine ore deposits *in* Wilson, M.E., ed., Structural geology of Canadian ore deposits: Montreal, Quebec, Canadian Institute of Mining and Metallurgy Symposium, Jubilee Volume, p. 442–456.
Elliot, S.R., 1984, Geochemical, mineralogical, and stable isotope studies at the Owl Creek mine, Timmins, Ontario: Unpublished B.Sc. thesis, Ottawa, Ontario, Carleton University, 110 p.
Evans, E.L., 1944, Porphyry of the Porcupine district, Ontario: Geological Society of America Bulletin, v. 55, p. 1115–1142.
Ferguson, S.A., 1968, Geology and ore deposits of Tisdale township: Ontario Department of Mines Geological Report 58, 177 p.
Fyon, J.A., and Crocket, J.H., 1982, Gold exploration in the Timmins district using field and lithogeochemical characteristics of carbonate alteration zones: Canadian Institute of Mining and Metallurgy Special Volume 24, p. 113–129.
Gray, M.D., 1994, Multiple gold mineralizing events in the Porcupine mining district, Timmins area, Ontario, Canada: Unpublished Ph.D. dissertation, Golden, Colorado, Colorado School of Mines, 220 p.
Griffis, A.T., 1968, Description of properties, McIntyre Porcupine Mines Limited: Ontario Department of Mines Geological Report 58, p. 122–130.
Gross, G.A., 1988, Gold content and geochemistry of iron-formation in Canada: Geological Survey of Canada Paper 86-19, 54 p.
Groves, D.I., Phillips, G.N., Ho, S.E., Houstoun, S.M., and Standing, C.A., 1987, Craton-scale distribution of Archean greenstone gold deposits: Predictive capacity of the metamorphic model: Economic Geology, v. 82, p. 2045–2058.
Hodgson, C.J., 1983, The structural and geological development of the Porcupine camp—a re-evaluation: Ontario Geological Survey Miscellaneous Paper 110, p. 211–225.
Holmes, T.C., 1948, Dome mine *in* Wilson, M.E., ed., Structural geology of Canadian ore deposits: Montreal, Quebec, Canadian Institute of Mining and Metallurgy Symposium, Jubilee Volume, p. 539–547.
—— 1968, Description of properties, Dome Mines Limited: Ontario Department of Mines Geological Report 58, p. 82–98.
Hurst, M.E., 1939, Porcupine area, District of Cochrane, Ontario: Ontario Department of Mines Map 47a.
Hutchinson, R.W., 1993, A multi-stage, multi-process genetic hypothesis for greenstone-hosted gold lodes: Ore Geology Reviews, v. 8, p. 349–382.
Hutchinson, R.W., and Viljoen, R.P., 1988, Re-evaluation of gold source in Witwatersrand ores: South Africa Journal of Geology, v. 91, p. 157–173.
Jones, W.A., 1968, Description of properties, Hollinger Consolidated Gold Mines Limited: Ontario Department of Mines Geological Report 58, p. 102–115.
Karvinen, W.O., 1982, Geology and evolution of gold deposits, Timmins area, Ontario:. Canadian Institute of Mining and Metallurgy Special Volume 24, p. 101–112.
Kerrich, R., and Hodder, R.W., 1982, Archean lode gold and base metal deposits: Evidence for metal separation into independent hydrothermal systems: Canadian Institute of Mining and Metallurgy Special Volume 24, p.144–160.
Kingston, D.M., 1987, Geology and geochemistry of the Owl Creek gold deposit, Timmins, Ontario: Unpublished M.Sc. thesis, Ottawa, Ontario, Carleton University, 108 p.
Kusic, A., and Olson, P.E., 1990, Falconbridge Hoyle mine, Whitney township: Geological Survey of Canada Open File 2161, p. 110–113.
Lickley, W.P., 1985, Geochemistry and petrography of the greywacke wallrock hosting the Three Nations gold-quartz vein system, Pamour number one mine, Timmins, Ontario: Unpublished M.Sc. thesis, Sudbury, Ontario, Laurentian University, 71 p.
Lorsong, J., 1975, Stratigraphy and sedimentology of the Porcupine Group, Northeastern Ontario: Unpublished B.Sc. thesis, Toronto, Ontario, University of Toronto, 45 p.
Marmont, S., and Corfu, F., 1989, Timing of gold introduction in the Late Archean tectonic framework of the Canadian Shield: Evidence from U-Pb zircon geochronology of the Abitibi subprovince: Economic Geology Monograph 6, p. 101–111.
Mason, R., and Melnik, N., 1986a, The McIntyre-Hollinger investigation, Timmins, Ontario: A gold dominated porphyry copper system: Geological Survey of Canada Paper 86-1B, p. 577–583.
——1986b, The anatomy of an Archean gold system—the McIntyre-Hollinger Complex at Timmins, Ontario, Canada, *in* Macdonald, A.J., ed., Gold '86: Willowdale, Ontario, Konsult International, p. 40–55.
Mason, R., Melnik, N., Edmunds, C.F., Hall, D.J., Jones, R., and Mountain, B., 1986, The McIntyre-Hollinger investigation, Timmins, Ontario: Stratigraphy, lithology, and structure: Geological Survey of Canada Paper 86-1B, p. 576–575.
Mason, R., Brisbin, D.I., and Aitken, S.A., 1988, The geological setting of deposits in the Porcupine mining camp: Ontario Geological Survey Miscellaneous Paper 140, p. 133–145.
McAuley, J.B., 1983, A petrographic and geochemical study of the Preston, Preston West, and Paymaster Porphyries, Timmins, Ontario: Unpublished M.Sc. thesis, Sudbury, Ontario, Laurentian University, 118 p.
Melnik-Proud, N., 1992, The geology and ore controls in and around the McIntyre mine at Timmins, Ontario, Canada: Unpublished Ph.D. dissertation, Kingston, Ontario, Canada, Queens University, 353 p.
Moore, D.W., 1977, Geology and geochemistry of a gold-bearing iron formation and associated rocks, Back River, Northwest Territories: Unpublished M.Sc. thesis, Toronto, Canada, University of Toronto, 186 p.

Piroshco, D.W., and Kettles, K., 1988, Geology of Tisdale and northern Whitney townships—project number 87-15: Ontario Geological Survey Miscellaneous Paper 137, p. 197–205.

——1991, Structural geology of Tisdale and northern Whitney townships, Abitibi greenstone belt, District of Cochrane, Northeastern Ontario: Ontario Geological Survey Open File Report 5768, 115 p.

Price, P., and Bray, R., 1948, Pamour mine *in* Wilson, M.E., ed., Structural geology of Canadian ore deposits: Montreal, Quebec, Canadian Institute of Mining and Metallurgy Symposium, Jubilee Volume, p. 559–565.

Proudlove, D.C., 1989, A comparison of concordant and discordant gold veins, Dome mine, South Porcupine, Ontario: Unpublished M.Sc. thesis, Golden, Colorado, Colorado School of Mines, 187 p.

Proudlove, D.C., Hutchinson, R.W., and Rogers, D.S., 1989, Multiphase mineralization in concordant and discordant gold veins, Dome mine, South Porcupine, Ontario, Canada: ECONOMIC GEOLOGY MONOGRAPH 6, p. 112–123.

Pyke, D.R., 1982, Geology of the Timmins area, District of Cochrane: Ontario Geological Survey Report 219, 141 p.

Pyke, D.R., Ayres, L.D., and Innes, D.G., 1971, Map 2205-Timmins-Kirkland Lake: Ontario Division of Mines, Geological Compilation Series, Cochrane, Sudbury, and Timiskaming Districts, scale 1:253,440.

Rice, R., Born, P., and Donaldson, A., 1992, Archean sedimentology and stratigraphy: Dore metasediments, Michipicoten greenstone belt; Timiskaming and Porcupine metasediments, Abitibi greenstone belt: Ontario Geological Survey Miscellaneous Paper 159, p. 3–16.

Robert, F., and Poulsen, K.H., 1997, World-class Archaean gold deposits in Canada: An overview: Australian Journal of Earth Sciences, v. 44, p. 329–351.

Roberts, R.G., 1981, The volcanic-tectonic setting of gold deposits in the Timmins area, Ontario: Ontario Geological Survey Miscellaneous Paper 97, p. 16–28.

Rogers, D.S., 1982, The geology and ore deposits of the no. 8 shaft area, Dome mine: Canadian Institute of Mining and Metallurgy Special Volume 24, p. 161–168.

Rye, K.A., 1987, Geology and geochemistry of the Hoyle Pond gold deposit, Timmins, Ontario: Unpublished M.Sc. thesis, London, Ontario, University of Western Ontario, 220 p.

Saager, R., Meyer, M., and Muff, R., 1982, Gold distribution in supracrustal rocks from Archean greenstone belts of southern Africa and from Paleozoic ultramafic complexes of the European Alps: Metallogenic and geochemical implications: ECONOMIC GEOLOGY, v. 77, p. 1–24.

Smith, T.J., Cloke, P.L., and Kesler, S.E., 1984, Geochemistry of fluid inclusions from the McIntyre-Hollinger gold deposit, Timmins, Ontario, Canada: ECONOMIC GEOLOGY, v. 79, p. 1265–1285.

Walsh, J.F., Kesler, S.E., Duff, D., and Cloke, P.L., 1988, Fluid inclusion geochemistry of high-grade, vein-hosted gold ore at the Pamour mine, Porcupine Camp, Ontario: ECONOMIC GEOLOGY, v. 83, p. 1347-1367.

West, J.M., Wilson, S.D., Simunovic, M.R., and Olsen, P.E., 1990, Pamour # 1 mine: Geological Survey of Canada Open File 2161.

Wood, P.C., Burrows, D.R., Thomas, A.V., and Spooner, E.T.C., 1986, The Hollinger-McIntyre Au-quartz vein system, Timmins, Ontario, Canada: Geologic characteristics, fluid properties and light stable isotope geochemistry, *in* Macdonald, A.J., ed., Gold '86: Willowdale, Ontario, Konsult International, p. 103–109.

APPENDIX 1

Geochemical Analyses of Iron Formation, Pyritic Interflow Strata, and Sulfide Concentrates from Interflow Strata

Sample no.	% Sulfide	Au	Ag	Cu	Pb	Zn	Mo	As	Sb	Hg
Sulfide-poor iron-formation: Deloro Group										
TI-154-301	8	0.006	<1	99	18	73	3	6	1.3	0.016
TI-169-131	1	0.004	<1	26	6	49	2	5	0.2	0.009
TI-169-37.5	0.5	0.003	0.6	42	13	121	3	29	<.2	0.012
Average		0.004	0.267	56	12	81	3	13	0.6	0.012
Sulfide-rich iron-formation: Deloro Group										
TI-154-298	65	0.119	0.8	71	73	71	3	308	8.5	0.047
TI-156-190	40	0.046	24.4	54	122	128	<1	20	2.1	0.08
TI-156-194	35	0.135	47.4	141	286	5669	5	5	7.6	0.353
TI-169-44.5	90	0.217	1	20	62	41	<1	205	7.0	0.044
TI-169-47	90	0.136	0.3	31	34	43	<1	293	2.5	0.021
TI-169-136	55	0.025	<1	64	18	51	2	21	0.2	0.007
TI-331-486.7	95	0.069	1.5	25	85	27	<1	208	9.1	0.264
TI-331-489.4	60	0.099	4.4	22	136	56	<1	262	28.2	0.098
TI-333-464.2	90	0.007	0.2	112	18	454	<1	7	0.6	0.019
TI-333-477.2	60	0.112	0.4	78	50	31	<1	208	14.0	0.033
TI-1267-84.7	90	0.045						305	7.4	0.047
TI-1525-192	85	0.065	0.4	61	56	39	<1	269	10.0	0.033
Average		0.090	7.355	62	85	601	2	176	8.1	0.087
Sulfide-poor interflow strata: Tisdale Group										
H1507 240.8	3	0.074	0.5	225	41	813	5	170	16.0	0.25
H1509 182.2	2	0.158	1.2	535	56	1801	6	271	34.4	0.333
H1511 240.2	3	0.317	0.9	204	52	404	<1	222	39.4	0.087
OC8001 166.7	3	0.034	1	276	38	1083	6	185	12.0	1.085
OC8002 193.7	3	0.098	0.7	202	39	1124	3	206	7.6	0.578
OC8003 208.5	2	0.079	0.7	262	65	1146	4	222	6.3	0.755
OC8014 134.0	3	0.022	0.4	150	37	817	5	219	5.7	0.656
OC8015 135.2	1	0.03	0.7	180	35	506	3	177	9.1	0.536
OC8016 158.6	3	0.048	1	441	54	1526	10	277	16.0	1.118
OC8017 136.1	3	0.071	1.1	376	58	2552	8	283	20.0	1.251
OC8019 191.0	3	0.047	0.6	143	42	603	4	174	9.2	0.436
OC8020 184.6	10	0.037	<1	66	19	105	<1	92	4.5	0.081
Average		0.085	0.742	255	45	1040	5	208	15.0	0.597
Sulfide-rich interflow strata: Tisdale Group										
H1507 242.1	80	0.236	2.5	137	155	237	<1	273	64.1	0.355
H1520 250.0	90	0.342	2.8	49	113	126	3	306	94.7	0.122
Average		0.289	2.7	93	134	182	2	290	79.4	0.239
Sulfide concentrate from interflow strata: Tisdale Group										
H1507SC 242.1	100	0.683	4.5	279	227	371	1	479	105.0	0.578
H1520SC 250.0	100	0.321	2.9	36	119	85	<1	421	109.0	0.143
OC8014SC 134.0	100	0.288	2.9	387	164	936	2	820	56.9	1.419
OC8020SC 184.6	100	0.401	1.1	231	67	284	<1	530	23.9	0.401
Average		0.423	2.9	233	144	419	1	563	73.7	0.635

Values less than detection limit set to detection limit for calculation of averages

APPENDIX 2

Major Element Oxide Geochemical Data, Feldspar Porphyry and Quartz Feldspar Porphyry, Blueberry Hill Area, Dome Mine

Sample ID	Rock type	SiO_2	Al_2O_3	Fe_2O_3	MgO	CaO	Na_2O	K_2O	Total
FOB1	FP	67.36	15.98	2.88	1.80	1.33	5.38	2.08	96.81
FOB2	FP	67.05	16.63	2.37	1.75	2.11	5.09	2.28	97.28
FOB3	FP	64.06	15.54	2.34	1.64	2.44	4.72	2.37	93.11
FOB4	FP	64.01	16.27	3.28	1.79	1.53	5.82	1.42	94.12
FOB5	FP	64.04	15.91	2.49	1.68	2.68	4.43	2.21	93.44
FOB6	FP	63.40	17.02	2.83	1.78	1.53	5.83	2.00	94.39
FOB7	FP	64.87	17.22	2.85	1.75	2.48	5.53	1.73	96.42
FOB8	FP	64.08	17.12	3.05	1.80	3.41	4.72	1.96	96.14
FOB9	FP	65.36	15.85	2.71	1.80	2.20	4.86	2.27	95.05
BBH37	FP	65.64	16.29	2.27	1.23	2.38	5.17	2.09	95.06
BBH38	FP	65.41	16.04	2.40	1.09	4.66	5.24	2.07	96.91
Average		65.03	16.35	2.68	1.65	2.43	5.16	2.04	95.34
Standard deviation		1.29	0.57	0.33	0.25	0.95	0.46	0.27	1.46
BBH2	QFP	63.27	16.24	3.03	1.66	1.53	4.28	3.13	93.14
BBH3	QFP	61.75	15.85	2.57	1.58	2.45	5.00	2.61	91.81
BBH5	QFP	64.86	16.25	3.56	1.62	2.02	3.56	3.50	95.37
BBH7	QFP	66.04	17.88	1.71	1.44	2.10	4.41	3.52	97.10
BBH10	QFP	66.47	16.95	1.88	1.74	2.64	3.93	3.56	97.17
BBH11	QFP	66.77	16.17	2.02	1.47	3.58	4.72	2.91	97.64
BBH15	QFP	61.88	15.26	2.57	1.73	4.32	6.63	1.56	93.95
BBH16	QFP	59.01	14.70	2.78	1.64	3.35	4.72	2.47	88.67
BBH21	QFP	63.92	16.70	2.74	1.69	2.82	4.16	3.45	95.48
BBH24	QFP	58.35	13.72	7.84	1.04	2.34	5.20	1.89	90.38
BBH26	QFP	62.31	16.24	3.68	1.90	3.85	5.29	2.61	95.88
BBH52	QFP	65.36	16.22	2.37	2.07	2.16	4.32	2.84	95.34
FOB10	QFP	65.56	15.82	3.84	1.63	0.88	4.94	2.36	95.02
DDH24153 39.5-43	QFP	58.84	13.88	3.77	1.49	5.98	4.20	2.15	90.31
DDH24153 87-87.9	QFP	62.18	15.92	4.19	2.10	1.47	4.29	2.45	92.60
DDH24153 71-72.5	QFP	56.69	14.68	2.64	2.22	4.49	5.45	1.88	88.05
DDH24153 133-134.5	QFP	61.21	17.04	2.63	1.87	1.58	3.27	3.74	91.34
DDH24153 146-147	QFP	63.70	17.24	2.48	1.75	0.97	4.68	2.97	93.79
DDH24153 170-171	QFP	64.43	16.85	3.96	2.11	1.12	3.74	3.30	95.51
DDH24154 16-17.5	QFP	60.21	13.49	5.93	2.07	1.45	4.84	1.58	89.57
DDH24155 320.5-321.5	QFP	71.73	13.33	3.30	2.20	0.85	4.22	1.69	97.32
DDH24155 325-326	QFP	66.20	15.13	3.11	1.66	1.08	4.70	2.24	94.12
DDH24156 16-17	QFP	60.15	16.00	3.23	1.09	2.23	6.16	2.11	90.97
DDH24156 21-22.4	QFP	63.64	15.95	1.96	1.65	2.98	5.21	2.67	94.06
DDH24157 87.25-88.5	QFP	63.98	15.53	3.48	0.89	2.45	3.10	3.61	93.04
DDH24157 138.8-139.9	QFP	57.82	15.03	3.33	1.19	1.83	5.04	2.55	86.79
DDH24157 179.3-179.9	QFP	63.17	15.66	2.47	1.93	2.86	3.55	3.49	93.13
DDH24157 184.6-186	QFP	62.20	16.51	2.07	1.71	1.91	3.94	3.49	91.83
DDH24159 22.8-23.55	QFP	67.58	17.08	1.06	0.66	1.21	7.72	1.50	96.80
DDH24159 37.9-38.9	QFP	64.33	13.34	3.24	1.72	2.77	4.71	2.09	92.20
DDH24159 257.5-259	QFP	63.18	14.70	3.76	2.03	1.91	4.01	2.71	92.30
DDH24159 289.8-290.8	QFP	59.63	14.86	2.03	1.73	1.70	3.92	2.88	86.75
DDH24161 44-45.5	QFP	52.56	11.68	4.49	0.62	8.83	5.61	1.15	84.94
DDH24161 64.5-66	QFP	62.96	17.25	2.37	1.17	1.68	3.27	4.10	92.80
Average		62.70	15.56	3.12	1.62	2.51	4.61	2.67	92.80
Standard deviation		3.60	1.38	1.25	0.41	1.60	0.97	0.75	3.26

Abbreviations: FP = feldspar porphyry, QFP = quartz-feldspar porphyry